VOLUME 2: TABLE OF CONTENTS

APPENDIX I : BACKGROUND INFORMATION

In this appendix the information regarding the following subjects is presented:

- Summary of types of dams.
- Construction of earthfill embankment dams.
- Modelling of soil properties.
- Commonly applied limit equilibrium methods.
- Governing principles for modelling infiltration.
- Target reliabilities and expected performance levels.

I.1 The Main Types of Dams Constructed

The four main dam types constructed are:

I.1.1 Embankment dams

They are the only dams not constructed using concrete. The majority of these dams are constructed using only natural and fabricated materials, such as soil, clay or rock. ICOLD defines these types of embankment dam as '*any dam constructed of excavated materials placed without addition of binding materials other than those inherent in the natural material. The materials are usually obtained at or near the damsite*' as cited by Graham (1997). The main advantage of embankment dams is that they can be constructed on a variety of foundations, ranging from weak unconsolidated glacial deposits to strong sedimentary, crystalline igneous and metamorphic rocks (Wahlstrom, 1974), as they exert less pressure on the foundations. When designing such dams, their

overall size and the amount of local material available for its construction are also considered.

I.1.2 Arch dams

These dams are constructed using concrete and predominately built in steep, narrow, valleys where the valley's walls and foundations are of good solid rock (Creager, Justin & Hinds, 1945a). To be able to resist the force of the water stored directly behind the dam, the curve of the arch faces the reservoir (Hirschfeld & Poulos, 1973). Here the force of the water acting on the abutments is greatest near the valley walls than the valley floor.

I.1.3 Gravity dams

Can be constructed in either narrow or wide valleys and are the largest and heaviest of any constructed concrete or masonry dam (Smith, 1971). As they rely on their overall weight for stability against sliding and overturning, the dam's embankment has a large base. The main drawback of this type of dam is that it can only have a solid rock foundation.

I.1.4 Buttress dams

Like the gravity dam, the buttress dam's design also makes it ideal for construction in narrow or wide valleys. This type of dam also uses the least amount of concrete or masonry material in the dam's wall, due to the free space between each buttress support (Agate, 2001). These supports provide the strength required to resist the water's force from causing the dam to slide and overturn. This design is ideal where materials are scarce or expensive to produce. Further classification of these types of dams is also reflected by the materials used (soil, rockfill, concrete, masonry, etc.) and the dam's overall size (dependent on the dam's hydraulic components, purpose of the dam, reservoir's maximum capacity, etc.). With every dam construction, the engineers have to take into consideration its final location and surrounding environment, the overall size of the dam, the type of materials used in the embankment's construction (Wahlstrom, 1974) including the total cost of the dam's construction.

I.2 Types of Embankment dams

The most commonly constructed embankment dams are lined, zoned, diaphragm and homogeneous embankments.

I.2.1 Lined embankment

A lined embankment incorporates an impermeable lining on both the upstream slope and floor bed of the reservoir to ensure that there is minimal deterioration due to seepage and erosion (Kennard, Hopkins & Fletcher, 1996). Construction of this embankment design is only when the soil of the embankment's foundation and reservoir is permeable to a depth in excess of 4m. This embankment deign is also very costly, especially if in the future, any remedial or maintenance work has to be carried out. Therefore, this type of embankment only considered when there is no other feasible alternative.

I.2.2 Zoned embankment

A zoned embankment incorporates a core, or seepage barrier, within the central part of the embankment (Kennard, Hopkins & Fletcher, 1996). The central core can be composed of either an impermeable, or permeable but more stable, soil type compared to the rest of the embankment fill (Stone, 2003). If the zoned embankment is designed using a seepage barrier, the barrier has to be built using an impermeable type of material. This embankment design is preferred where there is a sufficient supply of different soil types at the dam site. As defined by Stephens (2010) zoned dams are *'constructed of varying soil materials, differentiated according to position and role in the structure'* (p.100). Figure I.1 shows a simple cross sectional diagram of this type of embankment design.

To ensure that there is minimal seepage through the embankment the base of the core, or seepage barrier, is twice that of the embankment's maximum height (Creager, Justin & Hinds, 1945a). Therefore, they will retain any water that has seeped through the embankment from the reservoir and its shoulders will stabilize the core. This means that

the slope protection, vegetation, on the embankment's surface only has to protect the slopes from erosion or deterioration.

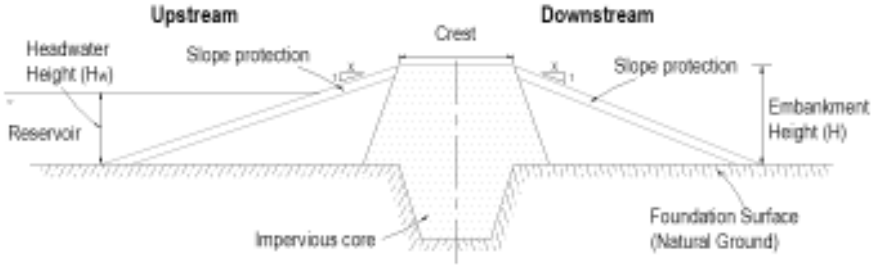

Figure I.1 Cross sectional diagram of a zoned embankment

I.2.3 Diaphragm embankment

This type of embankment, Figure I.2, comprises of a thin core or diaphragm on the upstream slope, constructed of an impermeable material such as bentonite concrete (Stone, 2003). The thickness of the impervious material is solely dependent on the height of the embankment. This type of embankment is only constructed when there is an insufficient supply of impermeable soil with which to construct the core of a zoned embankment.

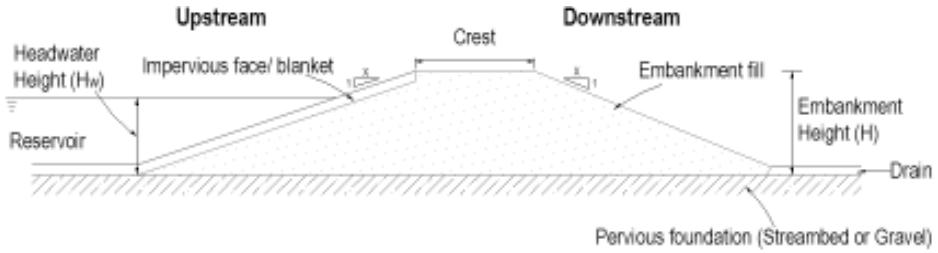

Figure I.2 Cross section of a typical diaphragm embankment design

The advantage of the diaphragm embankment is that there does not have to be an impervious layer below the embankment for it to be constructed. This type of embankment can also be modified and subsequently used where there appears to be an impervious layer at the foundation's surface. As the diaphragm embankment requires an impervious blanket on the upstream face, there are high costs involved in both building and maintaining the embankment. It is usually advisable to use a completely different design when constructing the embankment, or find a more practical dam site. As outlined by Kennard, Hopkins and Fletcher (1996) the diaphragm embankment usually applies to larger embankments that have a maximum height of 8m. However when the

supply of impervious soil is very limited, and both homogeneous and zoned embankments are unsuitable, then a diaphragm embankment can be constructed.

I.2.4 Homogeneous embankment

Homogeneous embankments, Figure I.3, are constructed using only one type of material, which is sufficiently impervious to reduce the effect of seepage through the embankment during the dam's lifetime. To ensure that the embankment fill behaves in a consistent manner throughout the embankment, the material used for the embankment fill should come from the same source (Stone, 2003).

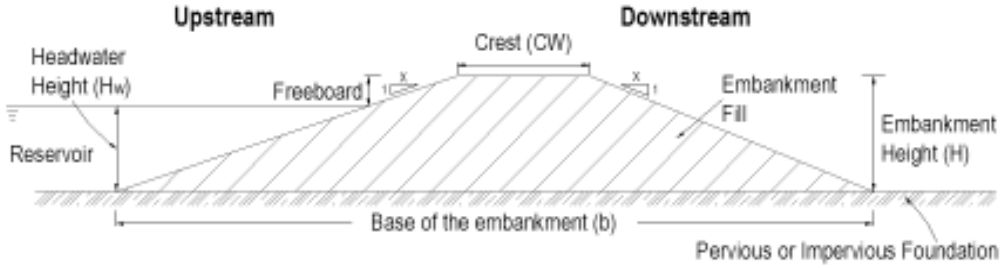

Figure I.3 Cross sectional diagram of a homogeneous embankment

I.3 Summary of Earthfill Embankment Dam Construction

Figure I.4 shows the plan of a simple arbitrary earthfill dam and its corresponding reservoir (Kennard, Hopkins & Fletcher, 1996). As shown in Figure I.4, the total area of the foundation is from the right abutment to the left abutment and covers the entire plan of the dam. As stated by Kennard, Hopkins and Fletcher (1996) when choosing the dam site, the foundation must be of adequate strength, and be sufficiently firm, to hold the weight of both the embankment and reservoir when filled to its maximum capacity. This is to ensure that there is sufficient resistance to avoid sliding of the embankment. Therefore, during the design stage the material composition and firmness of the foundation are also analysed, as they can vary at different locations altering the foundation's structural reliability. Most soil types have sufficient strength to bear the weight of an arbitrary small homogeneous earthfill dam. However, they should have a relatively low permeability to ensure little or no water seeps through the foundation under the reservoir or through the embankment into the foundation. At the design stage, the angle of the foundation's incline must also be included, as it also has an effect on

the overall stability of the embankment. For it not to affect the embankment's stability, the foundation must have a gradient less than 1V: 10H, or 5˚. If the foundation has a steeper incline, then it is excavated to ensure its angle does not exceed 5˚ (Kennard, Hopkins & Fletcher, 1996).

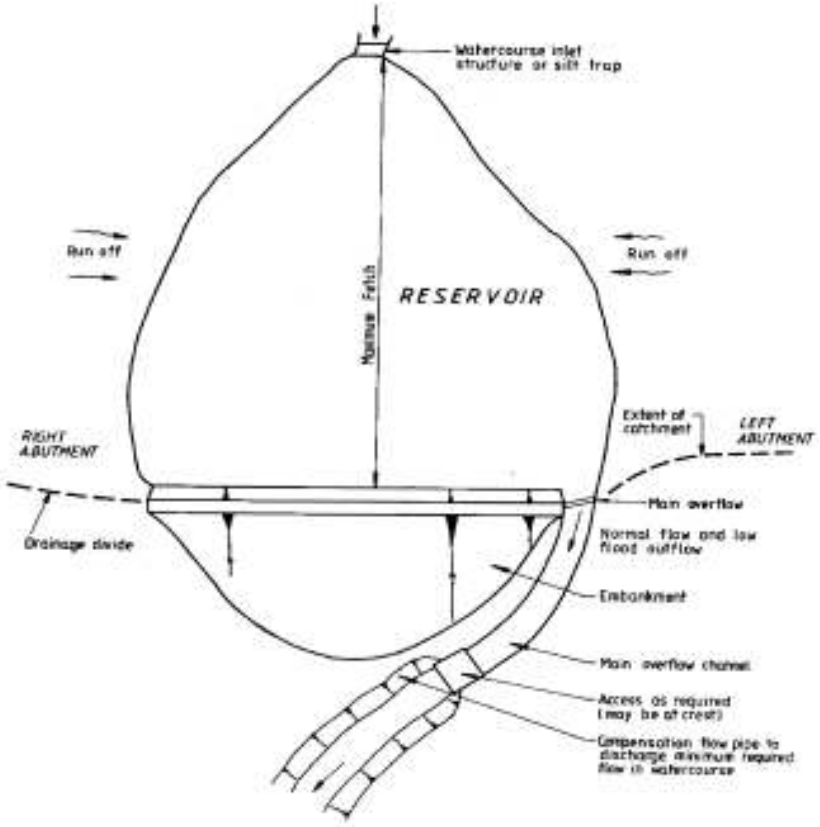

Figure I.4 Plan of a generic earthfill embankment dam and its reservoir[1]

I.3.1 Local materials considered for homogeneous earthfill embankments

When constructing any homogeneous earthfill embankment, the physical and mechanical properties of the locally sourced material and the surrounding climate conditions must be analysed. Tancev (2005) acknowledged that it is possible to use natural cohesive and non-cohesive soils when constructing an earthfill embankment, which do not contain water-soluble chlorides or more than 5 % sulphate-chloride salts, no more than 2% sulphate salts and no more than 5% insoluble organic matter. Table I.1 summarises the principal physical and mechanical characteristics of the local material used to construct any arbitrary homogeneous earthfill embankment.

[1] Extracted from Kennard, Hopkins & Fletcher (1996)

Table I.1 Soil types and their properties used for homogeneous earthfill embankments[2]

Homogeneous Earthfill Embankments		
Nature	→	Clay/Silts
Particle range	→	< 0.1mm
Strength	→	Low - medium
Permeability	→	Very low

I.3.2 Construction of earthfill embankments

One of the most common methods used to construct any earthfill embankment is by successively compacting horizontal layers of soil. For each soil layer, the first step is to spread the soil evenly along the full length of the embankment and then fully compact it in a continuous process. This is to avoid any discontinuities occurring that could lead to:

- Areas of weakness within the embankment fill.
- Discrepancies during settlement of the embankment fill.
- Potential leakages through the embankment fill.

As each soil layer is compacted, the air voids within the soil either shrink or disappear due to the force exerted on the soil. This causes the soil's structure to change, resulting the strength of the embankment fill to improve as the soils permeability is reduced (Agrawal, 2000). Since the soil's optimum moisture content also significantly affects the overall behaviour and maximum density of the embankment fill, the soil used must be free from lenses pockets, organic material and any other imperfections (KBR, 2002). Despite taking all the necessary steps during the embankment's construction, the embankment fill will continue to undergo some physical and chemical changes during the dam's lifetime. For this reason, when the embankment is initially constructed it is overfilled beyond its original design criteria by approximately 5% and then trimmed down to the specified dimensions (Kennard, Hopkins & Fletcher, 1996).

I.3.3 Settlement of the embankment during its lifecycle

All embankments undergo some form of settlement regardless of their construction and the composition of their foundation. Settlement is due to either elastic distortion or consolidation of the embankment fill (Creager, Justin & Hinds, 1945b). It can also be affected by natural environmental conditions or those imposed by the construction and

[2] Extracted from Tancev (2005: p.117)

operation of the dam. Elastic distortion occurs in all structures and is proportional to the load of the embankment. This form of settlement is relatively small and occurs rapidly compared to consolidation settlement. In comparison, settlement due to consolidation is the primary cause of settlement of earthfill embankments or those constructed on an earth foundation. Smout and Shaw (1999) define consolidation as the change in the soil's volume caused by changes in the void ratios, which also affects the embankment's crest height. Changes in the crest height can develop slowly and over any length of time, even without the operator or maintenance engineer noticing that there is a reduction in the embankment's height or freeboard. Therefore, when constructing the embankment and its foundation settlement is considered. This includes increasing the height of the embankment at the design stage and once constructed periodically measuring the embankment's height.

I.4 Modelling of Soil Properties

Soil is composed of three principal phases, identified as solids composed of mineral particles (such as disintegrated rock and decayed vegetation), gas or air and liquid which is almost always water (Whitlow, 1995; Liu & Evett, 2006). Figure I.5 shows the soil-phase model including the masses and volumes of the three phases. The composition of the soil is important, as when the soil is (Sutton, 1993):

- Dry, its voids are full of air.
- Fully saturated, its voids are full of water.
- Partially saturated, its voids contain water and air.

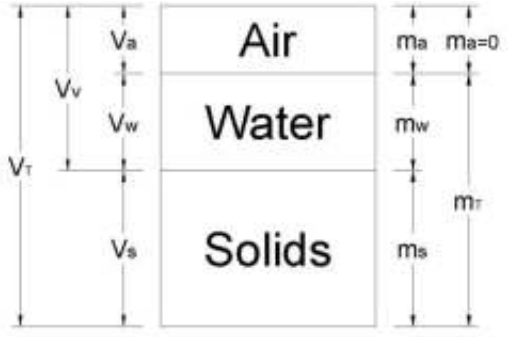

KEY

V_s	Volume of solids
V_a	Volume of air
V_w	Volume of water
V_v	Volume of voids
V_T	Total volume
m_s	Mass of solids
m_a	Mass of air
m_w	Mass of water
m_T	Total mass of sample

Figure I.5 Soil-phase model[3]

[3] Extracted from Liu and Evett (2006).

From the soil-phase model, the following key parameters of the soil can be derived (Barnes, 2000):

- Void ratio (e)
- Porosity (n_s)
- Moisture content (θ)
- Degree of saturation or saturation level (S_r)
- Specific gravity (G_s)

The relationship between the volume of voids and solid soil particles are defined by the void ratio and porosity of the soil, which are found using the following equations (Liu & Evett, 2006).

Void ratio: $$e = \frac{V_v}{V_s} = \frac{n_s}{1 - n_s} \qquad 0 < e \ll \infty \qquad \text{(I.1)}$$

Porosity: $$n_s = \frac{V_v}{V_T} = \frac{e}{1 + e} \qquad 0 \leq n_s \leq 1 \qquad \text{(I.2)}$$

The moisture content, Eqn. (I.3), indicates the amount of water present in the soil. This is not a constant parameter, and may vary due to changes in the soil's surroundings over time. The soil's degree of saturation, Eqn. (I.4), defines the ratio between the volume of water in the void space and the total volume of voids in the soil. From Eqn. (I.5) the soil's specific gravity can be defined. However the equation is not often applied, as the specific gravity for most soils is valued between 2.60 and 2.77 (Bowles, 1984).

Moisture content: $$\theta = \left(\frac{m_w}{m_s} \right) \cdot 100 \qquad 0 \leq \theta \ll \infty \qquad \text{(I.3)}$$

Degree of saturation: $$S_r = \left(\frac{V_w}{V_V} \right) \cdot 100 \qquad 0 \leq S_r \leq 100 \qquad \text{(I.4)}$$

Specific gravity: $$G_s = \left(\frac{m_s}{V_s \cdot \rho_w} \right) \qquad \text{(I.5)}$$

where: ρ_w represents the density of water.

By establishing the soil's physical properties, an adequate representation of its mechanical behaviour can be derived using standard formulae.

I.5 Summary of the Most Commonly Applied Stability Methods for Determining Slope Instability

The most common limit equilibrium methods are the circular arc method; method of slices; finite element method and the sliding block method. Here the circular arc method, finite element method and method of slices are summarised.

I.5.1 Circular arc method

Craig (1992) and Whitlow (1995) both indicate that when applying the circular arc method the slope's failure surface is considered rotational and not translatory. Figure I.6 shows a simple sketch of the circular arc method. It assumes the soil's shear strength, along the failure plane, is governed by the linear Mohr-Coulomb relationship between the shear strength and normal stress on the slope's failure surface. This is the simplest method that can be applied, but the analysis has to be repeated several times, to obtain the slope's minimum factor of safety.

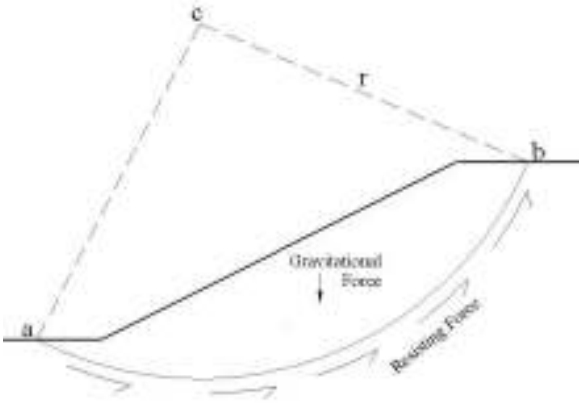

Figure I.6 Sketch of the circular arc method

In this particular method, the centre of the circular arc (failure surface) is taken at a point above the slope (point C), see Figure I.6. In order to obtain the slope's critical failure surface, this methodology is performed on different failure surfaces within the slope. Each failure surface will have a different radius and subsequently a different factor of safety. The failure surface with the lowest factor of safety is deemed the critical failure surface for that slope. However, Whitlow (1995: p.333) states that *'for*

long term problems, where changes in conditions may occur long after the end of construction a form of effective stress analysis is required.' Therefore, stability of the slope must be analysed in terms of its effective stresses and changes in pore water pressure. This can be carried out by simply applying the method of slices.

I.5.2 Method of slices

This is the most commonly applied limit equilibrium method when analysing the stability of a slope, as stated by Sengupta and Upadhyay (2005), and Hammouri, Malkawi and Yamin (2008). Like the circular arc method, it also assumes that the slope's failure surface is rotational. When considering the method of slices there are several methodologies, which can be applied. Such methods include Fellenius (Swedish) method, Bishop's method, Janbu's method, etc., (Fell, MacGregor & Stapledon 1992; Griffiths & Lane 1999). These methods all follow the same approach where the soil mass above the assumed failure surface is divided into vertical slices, and the stability of each individual slice is calculated. The method of slices model is illustrated in Figure I.7.

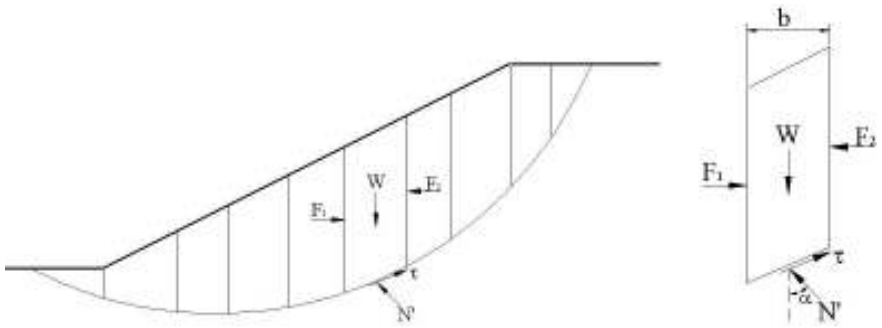

Figure I.7 Sketch of the Method of Slices

Fellenius (1936) first developed the method of slices further, and is known as the Fellenius Method or the Swedish Method of Slices (Atkinson, 1993). Fellenius's simplified method assumes that the forces acting on the individual slice are parallel to the base of the slice, or the base of the slope's failure surface (Liang, Nusier & Malkawi, 1999) as shown in Figure I.7. The interslice forces (F_1 and F_2) acting on the sides of each slice are assumed to be equal and opposite ($F_1 = F_2$), thus cancelling the other out normal to the slope's failure surface (Whitlow, 1995; Craig, 1992). However, this specific method tends to produce a low factor of safety.

Bishop (1955) developed the method of slices even further establishing a more accurate factor of safety, known as the Simplified Bishop Method, where the interslice forces also act normal to the slice. It is assumed *'that the resultant of the interslice forces is horizontal…and each slice is statically determinate'* Atkinson (1993: p.249). Using an iterative process, the Simplified Bishop Method can rapidly determine the slope's factor of safety by establishing its critical failure surface, due to the repetitiveness of the applied equations and by examining a number of possible failure surfaces (Smith, 1982). The complexity of the slope's geometry and soil properties can also be easily implemented into The Bishop Method (Smith, 1982; Tancev, 2005). This method is routinely used in computer programs, as the slope can be divided into different soil layers and any number of slices. However, Bishop's Method still underestimates the factor of safety (Craig, 1992). This method is therefore still an approximation to a degree, as it does not consider all conditions requiring a number of assumptions in the methodology.

Janbu's Simplified Method differs from the other method of slices, as it can determine slope stability for non-circular failure surfaces. For this method, correction factors are sometimes applied to the calculated factor of safety and account for the assumed horizontal interslice forces (Janbu, 1973). Zhan, Zhang and Chen (2006) implemented this method to establish the factor of safety for a specific earthfill slope when its embankment's reservoir level is changed. However, the factor of safety obtained from the Simplified Janbu Method must be reviewed with care, when verifying whether a correction factor was implemented into the methodology (USACE, 2003).

The disadvantage of these limit equilibrium methods is that they do not easily consider seepage flow through the slope (Michalowski, 1995). Baker (2006: p.276) also states that these *'limit equilibrium methods are based on kinematical and static assumptions which cannot be rationally justified.'* These methods also assume that above the failure surface, the embankment fill can be easily divided into slices. It is these forces, which differentiate the different limit equilibrium methods (Griffiths & Lane, 1999). The results obtained are therefore dependent on the assumptions and conditions applied to the slope stability model. An alternative to the above-mentioned methods is to simulate slope failure using numerical finite element methods.

I.5.3 Finite element method

Over recent years, finite element methods have become more dominant in slope stability analysis. This form of methodology can easily incorporate the complexity of the soil properties within different soil layers, such as variations in the soil's type, unit weight, cohesion and internal friction, and the key parameters relating to the slope's geometry (Möllmann and Vermeer, 2007). By meshing the slope, the failure surface will be defined by the weak soil layers rather than the slope's predefined rotational failure surface. Thus providing the displacement patterns where potential failure mechanisms could develop within the slope. When meshing the slope, smaller elements are used where the greatest changes will occur in the slope's soil behaviour. When considering unsaturated soil the size of the elements is important (Smith, 2003). The boundary conditions can also have a significant effect on the slope's factor of safety and must be carefully identified on the finite element mesh.

There are many finite element programmes used in slope stability analysis, but the leading slope stability program is SLOPE/W, which can determine the factor of safety of earth and rock dams. It establishes the critical failure surface for both simple, and complex, slip failure surfaces using modern limit equilibrium software (Krahn, 2004). However, due to the complexity of the finite element method, it is not ideal for obtaining the slope's factor of safety when considering uncertainties associated with the embankment dam.

I.6 Governing Principles for Modelling Infiltration

To quantify the infiltrated depth of water through the soil, Horton's and Philip's equation can be applied. These empirical methods are all based on Richard's equation, which is the partial differential equation for one-dimensional vertical flow developed by Richards (1931) to examine infiltration in unsaturated soils (Chow, Maidment & Mays, 1988).

I.6.1 Richard's equation

Richard's equation, Eqn. (I.6), is derived from Darcy's law and the mass conservation law of water flow (Richards, 1931) and is considered the governing differential equation of infiltration in unsaturated soils (Chow, Maidment & Mays, 1988).

$$\frac{d\theta}{dt} = \frac{\partial}{\partial z}\left(K\frac{\partial \psi}{\partial \theta}\frac{\partial \theta}{\partial z} + K \right) = \frac{\partial}{\partial z}\left(D\frac{\partial \theta}{\partial z} + K \right) \tag{I.6}$$

where: θ = Measured moisture content; K = Hydraulic conductivity; $D = K\frac{\partial \psi}{\partial \theta}$ = Soil water diffusivity.

I.6.2 Horton's equation

The Horton equation (1933, 1939), Eqn. (I.7), was developed from Richard's equation where K and D, as defined in Eqn. (I.6), are constants acting independently to the soil's moisture content (Chow, Maidment & Mays, 1988). This was proved by Eagleson (1970) and Raudkivi (1979) and is considered an empirical formula. In this case, the soil's hydraulic conductivity and soil water diffusivity are taken as constant values, independent of the soils' moisture content (Hsu, Ni & Hung, 2002). It was Horton who noticed that infiltration has an initial rate (f_o), which exponentially decreases until it reaches a minimum constant infiltration rate (f_c).

$$f_p(t) = f_c + (f_0 - f_c)e^{-\lambda t} \tag{I.7}$$

where: f_p = Infiltration capacity; λ = Decay constant; t = Time.

Horton also demonstrated that when the rainfall rate (i) exceeds the soil's infiltration rate (f), the water will infiltrate the soil's surface at a rate that will generally decreases with time (Bedient, Huber & Vieux, 2008). As stated by Chow, Maidment and Mays (1988), the results obtained are only for the rate of moisture diffusion at the soil's surface. The advantage of this methodology is that it provides a good fit to the implemented data. However, the disadvantage, as noted by Bedient, Huber and Vieux (2008), is that the infiltration capacity decreases as a function of time irrespective of the actual amount of water available for infiltration. In other words, ponding is assumed and the infiltration capacity will decrease regardless whether the rainfall intensity exceeds f_0. Also, this method is time consuming, as the variables, λ, f_c, and f_o must be calculated

from experimental data rather than measured in a laboratory (Chow, Maidment & Mays, 1988).

I.6.3 Philip's equation

An alternative method is Philip's equation, Philip (1957), which is the basis for understanding water movement through different soil types. Philip applied the Boltzmann transformation to solve Richard's equation, to yield an infinite series for calculating the cumulative infiltration, F(t), as formulated in Eqn. (I.8). Unlike Horton's equation it is assumed that the hydraulic conductivity (K) and diffusivity (D) vary with the soil's moisture content (Chow, Maidment & Mays, 1988).

$$F(t) = St^{\frac{1}{2}} + Kt \tag{I.8}$$

where: S = Sorptivity, which is a function of the soil's wetting front suction head.

However, the general analytical results are meagre due to a very strong dependency on the moisture content on the diffusivity, which influences the soils' hydraulic conductivity (Parlange, 1971). Therefore, this particular method can only be taken as a rough first approximation, as the soil's diffusivity varies greatly with the soil's moisture content.

I.7 Target Reliability Indices and Expected Performance Levels

Table I.2 Target Reliability indices and expected performance levels according to U.S. Army Corps of Engineers (USACE) (1997: p.B-11)

Table B-1. Target Reliability Indices

Expected Performance Level	Beta	Probability of Unsatisfactory Performance
High	5	0.0000003
Good	4	0.00003
Above average	3	0.001
Below average	2.5	0.006
Poor	2.0	0.023
Unsatisfactory	1.5	0.07
Hazardous	1.0	0.16

Note: Probability of unsatisfactory performance is the probability that the value of performance function will approach the limit state, or that an unsatisfactory event will occur. For example, if the performance function is defined in terms of slope instability, and the probability of unsatisfactory performance is 0.023, then 23 of every 1,000 instabilities will result in damage which causes a safety hazard.

APPENDIX II : EQUATIONS FOR THE DOWNSTREAM SLOPE STABILITY MODEL

This appendix lists the detailed equations required to determine:

- The active earth pressure forces from the upstream slope acting on the downstream slope.
- The designated areas of the embankment fill used to identify the different unit weights of soil within the downstream slope.
- The vertical effective stresses on the downstream slope.

These equations are integral to carrying out the downstream slope stability model, using sliding block formulation, and the modified downstream slope stability model, using the advanced sliding block formulation, for precipitation effects (ASMP) as illustrated in Figures 2.9, *Chapter 2: Subsection 2.9.1*.

II.1 Downstream Slope Stability Model

II.1.1 Areas allocated for the unit weights of soil within the downstream slope

The following set of equations, Eqns. (II.1 to I.8), are used to determine the distribution of the unit weight of soil above, below and within the foundation of the downstream slope. The total area of the slope (A_{Td}) and foundation (A_{fd}) identified in Figure 2.10, *Chapter 2: Subsection 2.9.1*, are calculated using Eqns. (II.1 and II.2).

$$A_{Td} = \frac{1}{2} \cdot b_d \cdot H \tag{II.1}$$

$$A_{fd} = b_d \cdot H_f \tag{II.2}$$

where: H = Height of the embankment; H_f = Foundation height; b_d = Total base width of the downstream slope.

To simplify the calculations used to determine areas A_{1d} to A_{3d}, the trajectory of the idealised phreatic line is plotted as a straight line through the downstream slope, as shown in Figure 2.12 in *Chapter 2: Subsection 2.9.1.* To determine the area below the phreatic line (A_{1d}) and at the downstream toe (A_{2d}), Eqns. (II.3 and II.4) are applied. Thus, the total area above the phreatic line (A_{3d}) is established, Eqn. (II.5).

$$A_{1d} = \int_{b_{d2}}^{b_d} y \, dx = \frac{1}{3y_0}\left[\left(2y_0 b_d + {y_0}^2\right)^{\frac{3}{2}} - \left(2y_0 b_{d2} + {y_0}^2\right)^{\frac{3}{2}}\right] \tag{II.3}$$

$$A_{2d} = \frac{1}{2} \cdot b_{d2} \cdot H_4 \tag{II.4}$$

$$A_{3d} = A_{Td} - (A_{1d} + A_{2d}) \tag{II.5}$$

where: H_4 = Height of the phreatic line at the point where exits the downstream slope; b_{d2} = Width of the downstream toe; y_o is the horizontal distance between point A_1 and where it would intersect the foundation on the upstream side of the embankment, point B_1, see Figure 2.3 in *Chapter 2: Subsection 2.6.1*.

II.1.2 Total passive earth pressure force (P_{pD})

The total passive earth pressure force (P_{pD}) defines the force acting on the downstream slope from the foundation. By applying the following equations, P_{pD} is established.

$$\sigma_{P_D}{}' = \sigma_{v3_d}{}'(K_p) + 2c'\sqrt{K_p} \tag{II.6}$$

$$\sigma_{P_D} = \sigma_{P_D}{}' + u_{3d} \tag{II.7}$$

$$P_{pD} = \frac{1}{2} \cdot \sigma_{P_D} \cdot H_f \tag{II.8}$$

where: K_p = Coefficient of passive earth pressure; σ_{PD}'= Effective stress acting on the downstream slope; σ_{PD} = Stress acting on the downstream slope; H_f = Foundation height; c' = Cohesion.

II.1.3 Active earth pressure force (P_{XU}) of the upstream slope

To determine the total active earth pressure force (P_{XU}) acting on the downstream slope, from the upstream slope, the following stresses, effective stresses and pore pressures have to be established:

- The vertical effective stress (σ_{v1_u}', σ_{v2_u}' and σ_{v3_u}')
- The horizontal effective stresses (σ_{h1_u}', σ_{h2_u}' and σ_{h3_u}')
- The horizontal stresses (σ_{h1_u}, σ_{h2_u} and σ_{h3_u})

The first step is to determine the vertical effective stresses (σ_{v1_u}', σ_{v2_u}' and σ_{v3_u}') acting on the upstream slope. These are obtained by subtracting the pore pressures (u_{1_u}, u_{2_u} and u_{3_u}) from the vertical stresses (σ_{v1_u}, σ_{v2_u} and σ_{v3_u}), as equated in *Chapter 2: Subsection 2.9.1*.

$$\sigma_{v1_u}' = \sigma_{v1_u} - u_{1u} \quad \text{(II.9)}$$

$$\sigma_{v2_u}' = \sigma_{v2_u} - u_{2u} \quad \text{(II.10)}$$

$$\sigma_{v3_u}' = \sigma_{v3_u} - u_{3u} \quad \text{(II.11)}$$

Once the vertical effective stresses are calculated, the second step is to establish the horizontal effective stresses (σ_{h1_u}', σ_{h2_u}' and σ_{h3_u}') acting on the upstream slope. By applying Eqn. (2.23), *Chapter 2: Subsection 2.8.2.1*, the horizontal effective stresses are determined using the following set of equations.

$$\sigma_{h1_u}' = \sigma_{v1_u}'(K_a) - 2c'\sqrt{K_a} \quad \text{(II.12)}$$

$$\sigma_{h2_u}' = \sigma_{v2_u}'(K_a) - 2c'\sqrt{K_a} \quad \text{(II.13)}$$

$$\sigma_{h3_u}' = \sigma_{v3_u}'(K_a) - 2c'\sqrt{K_a} \quad \text{(II.14)}$$

where: $K_a = \left(\frac{1-\sin\varphi}{1+\sin\varphi}\right)$ = Coefficient of active earth pressure.

The final step, before the total active earth force is established, the horizontal stresses (σ_{h1_u}, σ_{h2_u} and σ_{h3_u}) must be calculated by simply adding the horizontal effective stresses to their corresponding pore pressures, Eqns. (II.15 to II.17).

$$\sigma_{h1_u} = \sigma_{h1_u}' + u_{1u} \quad \text{(II.15)}$$

$$\sigma_{h2_u} = \sigma_{h2_u}' + u_{2u} \quad \text{(II.16)}$$

$$\sigma_{h3_u} = \sigma_{h3_u}' + u_{3u} \quad \text{(II.17)}$$

Thus, the individual active earth pressure forces (P_{XU1}, P_{XU2} and P_{XU3}), Eqns. (II.18 to II.20), and the total active earth pressure force (P_{XU}), Eqn. (II.21), acting on the downstream slope from the upstream slope can be obtained.

$$P_{XU} = \frac{1}{2} \cdot \sigma_{h1_u} \cdot \left(H - H_{av_u} \right) \tag{II.18}$$

$$P_{XU2} = \left(\frac{\sigma_{h1_u} + \sigma_{h2_u}}{2} \right) \cdot H_{av_u} \tag{II.19}$$

$$P_{XU3} = \left(\frac{\sigma_{h2_u} + \sigma_{h3_u}}{2} \right) \cdot H_f \tag{II.20}$$

$$P_{XU} = P_{XU1} + P_{XU2} + P_{XU3} \tag{II.21}$$

II.1.4 Total effective weight (ω_{ed}) of the downstream slope

To determine the effective weight above (ω_{ed1}) and below (ω_{ed2}) the phreatic line of the slope and the effective weight of the slope's foundation (ω_{ed3}), Eqns. (II.22 to II.24) are applied. Subsequently, the total effective weight (ω_{ed}) of the downstream slope can be evaluated, Eqn. (II.25).

Above the phreatic line: $$\omega_{ed1} = \gamma_m (A_{3d}) \tag{II.22}$$

Below the phreatic line: $$\omega_{ed2} = (\gamma_{sub} A_{1d}) + (\gamma_m A_{2d}) \tag{II.23}$$

In the foundation: $$\omega_{ed3} = \gamma_{fd} (A_{fd}) \tag{II.24}$$

$$\omega_{ed} = \omega_{ed1} + \omega_{ed2} + \omega_{ed3} \tag{II.25}$$

II.2 Modified Downstream Slope Stability Model

II.2.1 Areas allocated for the unit weights of soil within the downstream slope

In order to determine the distribution of the different unit weights of soil, the areas allocated within the slope must first be established. By applying following set of equations, Eqns. (II.26 to II.29), the area of the newly saturated fill (A_{4d}) and the areas above (A_{3d}), and below (A_{1d} and A_{2d}), the phreatic line can be found. The total area of the downstream slope (A_{Td}) and its foundation (A_{fd}) are calculated using Eqns. (II.1 and II.2).

$$A_{1d} = \int_{b_{d2}}^{BD} y\,dx = \frac{1}{3y_0}\left[\left(2y_0 BD + {y_0}^2\right)^{\frac{3}{2}} - \left(2y_0 b_{d2} + {y_0}^2\right)^{\frac{3}{2}}\right] \quad \text{(II.26)}$$

$$A_{2d} = \frac{1}{2}\cdot b_{d2}\cdot H_4 \quad \text{(II.27)}$$

$$A_{4_d} = L_{dwn}\cdot\left(\frac{\left(\sqrt{H^2 + {b_d}^2}\right) + ED}{2}\right) \quad \text{(II.28)}$$

$$A_{3d} = A_{Td} - (A_{1d} + A_{2d} + A_{4d}) \quad \text{(II.29)}$$

where: BD is calculated using Eqn. (5.80) in *Chapter 5: Subsection 5.5.2.1*; b_{d2} using Eqn. (2.98) defined in *Chapter 2: Subsection 2.9.2.1*; y_o = Horizontal distance between points A_1 and B_1 (Figure 2.3, *Chapter 2: Subsection 2.6.1*); H_4 = Height of the phreatic line at the point where it interests the newly saturated fill (point F in Figure 5.11, *Chapter 5: Subsection 5.5.1.6.2*); H = Height of the embankment; b_d = Total base width of the downstream slope; ED is calculated using Eqn. (5.81) derived in *Chapter 5: Subsection 5.5.2.1*.

II.2.2 Active earth pressure force (P_{XU}) of the upstream slope

Before the total active earth pressure force (P_{XU}) acting on the downstream slope from the upstream slope can be calculated, the first step is to establish the vertical effective stresses (σ_{v1a_u}', σ_{v1b_u}', σ_{v2_u}' and σ_{v3_u}') by applying Eqns. (5.25 to 5.28), derived in *Chapter 5: Subsection 5.5.1.3*. Once the vertical effective stresses are obtained, the horizontal effective stresses (σ_{h1a_u}', σ_{h1b_u}', σ_{h2_u}' and σ_{h3_u}') can be found by applying the following equations.

$$\sigma_{h1a_u}' = \sigma_{v1a_u}'(K_a) - 2c'\sqrt{K_a} \quad \text{(II.30)}$$

$$\sigma_{h1b_u}' = \sigma_{v1b_u}'(K_a) - 2c'\sqrt{K_a} \quad \text{(II.31)}$$

$$\sigma_{h2_u}' = \sigma_{v2_u}'(K_a) - 2c'\sqrt{K_a} \quad \text{(II.32)}$$

$$\sigma_{h3_u}' = \sigma_{v3_u}'(K_a) - 2c'\sqrt{K_a} \quad \text{(II.33)}$$

where: $K_a = \left(\frac{1-\sin\varphi}{1+\sin\varphi}\right)$ = Coefficient of active earth pressure.

Subsequently the horizontal stresses (σ_{h1a_u}, σ_{h1b_u} σ_{h2_u} and σ_{h3_u}), Eqns. (II.34 to 5.37), can be found by adding the horizontal effective stresses and pore pressures (u_{1a_u}, u_{1b_u}, $u_{2_u}$and u_{3_u}), Eqns. (5.21 to 5.24) in *Chapter 5: Subsection 5.5.1.3*.

$$\sigma_{h1a_u} = \sigma_{h1a_u}' + u_{1a_u} \quad \text{(II.34)}$$

$$\sigma_{h1b_u} = \sigma_{h1b_u}{}' + u_{1b_u} \quad \text{(II.35)}$$

$$\sigma_{h2_u} = \sigma_{h2_u}{}' + u_{2_u} \quad \text{(II.36)}$$

$$\sigma_{h3_u} = \sigma_{h3_u}{}' + u_{3_u} \quad \text{(II.37)}$$

Thus, by applying the following equations, the individual active earth pressure forces (P_{XU1a}, P_{XU1a}, P_{XU2} and P_{XU3}) and total active pressure force (P_{XU}) acting on the downstream slope from the upstream slope can be obtained.

$$P_{XU1a} = \frac{1}{2} \cdot \sigma_{h1a_u} \cdot L_{up} \quad \text{(II.38)}$$

$$P_{XU1a} = \left(\frac{\sigma_{h1a_u} + \sigma_{h1b_u}}{2} \right) \cdot H_{x_U} \quad \text{(II.39)}$$

$$P_{XU2} = \left(\frac{\sigma_{h1b_u} + \sigma_{h2_u}}{2} \right) \cdot H_{av_u} \quad \text{(II.40)}$$

$$P_{XU3} = \left(\frac{\sigma_{h2_u} + \sigma_{h3_u}}{2} \right) \cdot H_f \quad \text{(II.41)}$$

$$P_{XU} = P_{XU1a} + P_{XU1b} + P_{XU2} + P_{XU3} \quad \text{(II.42)}$$

where: L_{up} = Vertical depth of infiltrated water through the upstream slope; H_{x_U} = Average height of the partially saturated fill $\left(H_{x_U} = H - H_{av_U} - L_{up}\right)$; H_{av_U}= Average height of the idealised phreatic line ($H_{av_U} = \frac{H_w + H_1}{2}$); H_f = Height of the upstream slope's foundation.

II.2.3 Total effective weight (ω_{ed}) of the downstream slope

The total effective weight of the downstream slope (ω_{ed}) is found by adding the effective weights (ω_{ed1a}, ω_{ed1b} and ω_{ed2}) in the slope with the effective weight of the slope's foundation (ω_{ed3}).

Above the phreatic line:

$$\omega_{ed1a} = \gamma_{sat}(A_{4d})$$
$$\omega_{ed1b} = \gamma_m(A_{3d}) \quad \text{(II.43)}$$

Below the phreatic line:

$$\omega_{ed2} = (\gamma_{sub} A_{1d}) + (\gamma_m A_{2d}) \quad \text{(II.44)}$$

In the foundation:

$$\omega_{ed3} = \gamma_{fd}(A_{fd}) \quad \text{(II.45)}$$

$$\omega_{ed} = \omega_{ed1a} + \omega_{ed1b} + \omega_{ed2} + \omega_{ed3} \quad \text{(II.46)}$$

APPENDIX III : SUMMARY OF DETERMINISTIC ANALYSIS FOR SLOPE STABILITY MODEL

III.1 Slope Stability Model

Summary of results relating to the physical embankment model, evaluated deterministically, in *Chapter 2: Subsection 2.10* using the upstream and downstream slope stability models.

III.1.1 Embankment constructed of London Clay

Tables III.1 to III.8 show the calculated vertical and horizontal stresses, effective stresses, pore pressures and total active and passive earth pressure forces applied to determine the factor of safety for the upstream and downstream slopes of the embankment constructed of London Clay. Eqns. (III.1 and III.2) show the calculated active and passive earth pressure coefficients.

$$\text{Active earth pressure coefficient} = K_a = \left(\frac{1-\sin\varphi'}{1+\sin\varphi'}\right) = \left(\frac{1-\sin 20}{1+\sin 20}\right) = 0.49 \qquad \text{(III.1)}$$

$$\text{Passive earth pressure coefficient} = K_p = \left(\frac{1+\sin\varphi'}{1-\sin\varphi'}\right) = \left(\frac{1+\sin 20}{1-\sin 20}\right) = 2.04 \qquad \text{(III.2)}$$

where: φ' = Angle of internal friction.

Table III.1 Pore pressures acting through the upstream slope, core and downstream slope

Pore pressure (u)		Units	Upstream	Core	Downstream
Above the phreatic line	u_1	kN/m^2	0.00	0.00	0.00
Below the phreatic line	u_2		13.59	11.84	8.89
Through the fill and foundation	u_3		18.49	16.75	13.79
Pore pressure in the vertical direction	u_v		127.36		96.10

Table III.2 Vertical stresses acting on the upstream slope, core and downstream slope

Vertical stress (σ_v)		Units	Upstream	Core	Downstream
Above the phreatic line	σ_{v1}	kN/m^2	27.45	30.48	39.38
Below the phreatic line	σ_{v2}		55.27	59.06	50.19
Through the fill and foundation	σ_{v3}		65.31	70.90	57.01

Table III.3 Vertical effective stresses acting on the upstream slope, core and downstream slope

Vertical effective stress (σ_v')		Units	Upstream	Core	Downstream
Above the phreatic line	σ_{v1}'	kN/m^2	27.45	30.48	39.38
Below the phreatic line	σ_{v2}'		41.68	47.22	41.30
Through the fill and foundation	σ_{v3}'		46.82	54.16	43.21

Table III.4 Horizontal effective stresses acting on the upstream slope, core and downstream slope

Horizontal effective stress (σ_h')		Units	Upstream	Core	Downstream
Above the phreatic line	σ_{h1}'	kN/m^2	6.46	7.94	12.31
Below the phreatic line	σ_{h2}'		13.44	16.15	13.25
Through the fill and foundation	σ_{h3}'		15.95	19.55	14.19

Table III.5 Horizontal stresses acting on the upstream slope, core and downstream slope

Horizontal stress (σ_h)		Units	Upstream	Core	Downstream
Above the phreatic line	σ_{h1}	kN/m^2	6.46	7.94	12.31
Below the phreatic line	σ_{h2}		27.02	27.99	22.14
Through the fill and foundation	σ_{h3}		34.45	36.30	27.98

Table III.6 The effective weight of soil in the upstream and downstream slopes

Effective weight of slope (ω_e)		Units	Upstream	Downstream
Above the phreatic line	ω_{e1}	kN/m	106.41	152.05
Below the phreatic line	ω_{e2}		145.42	93.71
Through the fill and foundation	ω_{e3}		90.38	81.82
Total Effective weight	ω_e		342.21	327.58

From Table III.6, the total vertical effective force (σ_F) and effective shear stress (σ_v') acting on the upstream and downstream slopes were obtained.

Upstream slope:

$$\sigma_{F_u} = \omega_{eu} = 342.21\ \text{kN/m}^2 \quad \text{(III.3)}$$

$$\sigma_{vu}' = \frac{\sigma_{Fu} - u_{vu}}{b_u} = \frac{342.21 - 127.36}{9} = 23.87\,\text{kN/m}^2 \quad \text{(III.4)}$$

Downstream slope:

$$\sigma_{F_d} = \omega_{ed} = 327.58\ \text{kN/m}^2 \quad \text{(III.5)}$$

$$\sigma_{vd}' = \frac{\sigma_{Fd} - u_{vd}}{b_d} = \frac{327.58 - 96.10}{12} = 19.29\,\text{kN/m}^2 \quad \text{(III.6)}$$

Table III.7 Active earth pressures from the core, upstream and downstream slopes

Active earth pressures (P_a)		Units	Upstream	Core	Downstream
Above the phreatic line	P_{a1}	kN per m length of dam	5.21	7.12	14.26
Below the phreatic line	P_{a2}		23.19	21.69	11.77
Through the fill and foundation	P_{a3}		15.37	16.07	12.53
Total active earth pressure	P_{aT}		43.77	44.88	38.55

Table III.8 Passive pressure: force acting on the slope from the embankment's foundation

Passive earth pressures (P_p)		Units	Upstream	Downstream
Effective earth pressure	σ_P'	kN/m^2	109.78	102.42
Horizontal passive earth pressure	σ_P		128.27	116.22
Passive earth pressure force	P_p	kN per m length of dam	32.07	29.05

III.1.2 Embankment constructed of Medium Silt

For this deterministic analysis, the embankment fill is composed of Medium Silt. Tables III.9 to III.16 show the calculated vertical and horizontal stresses, effective stresses, pore pressures and total active and passive earth pressure forces used to calculate the factor of safety for the upstream and downstream slopes. Eqns. (III.7 and III.8) show the calculated active and passive earth pressures coefficients.

$$\text{Active earth pressure coefficient} = K_a = \left(\frac{1-\sin\varphi'}{1+\sin\varphi'}\right) = \left(\frac{1-\sin 26}{1+\sin 26}\right) = 0.39 \quad \text{(III.7)}$$

$$\text{Passive earth pressure coefficient} = K_p = \left(\frac{1+\sin\varphi'}{1-\sin\varphi'}\right) = \left(\frac{1+\sin 26}{1-\sin 26}\right) = 2.56 \quad \text{(III.8)}$$

Table III.9 Pore pressures acting through the upstream slope, core and downstream slope

Pore pressure (u)		Units	Upstream	Core	Downstream
Above the phreatic line	u_1	kN/m^2	0.00	0.00	0.00
Below the phreatic line	u_2		13.59	11.84	8.89
Through the fill and foundation	u_3		18.49	16.75	13.79
Pore pressure in the vertical direction	u_v		127.36		96.10

Table III.10 Vertical stresses acting on the upstream slope, core and downstream slope

Vertical stress (σ_v)		Units	Upstream	Core	Downstream
Above the phreatic line	σ_{v1}	kN/m^2	30.16	33.48	43.27
Below the phreatic line	σ_{v2}		59.43	64.34	55.16
Through the fill and foundation	σ_{v3}		69.99	77.12	62.66

Table III.11 Vertical effective stresses acting on the upstream slope, core and downstream slope

Vertical effective stress (σ_v')		Units	Upstream	Core	Downstream
Above the phreatic line	σ_{v1}'	kN/m^2	30.16	33.48	43.27
Below the phreatic line	σ_{v2}'		45.84	52.50	46.27
Through the fill and foundation	σ_{v3}'		51.50	60.37	48.87

Table III.12 Horizontal effective stresses acting on the upstream slope, core and downstream slope

Horizontal effective stress (σ_h')		Units	Upstream	Core	Downstream
Above the phreatic line	σ_{h1}'	kN/m^2	11.78	13.07	16.89
Below the phreatic line	σ_{h2}'		17.90	20.50	18.07
Through the fill and foundation	σ_{h3}'		20.11	23.57	19.08

Table III.13 Horizontal stresses acting on the upstream slope, core and downstream slope

Horizontal stress (σ_h)		Units	Upstream	Core	Downstream
Above the phreatic line	σ_{h1}	kN/m^2	11.78	13.07	16.89
Below the phreatic line	σ_{h2}		31.49	32.34	26.96
Through the fill and foundation	σ_{h3}		38.60	40.32	32.87

Table III.14 The effective weight of soil in the upstream and downstream slopes

Effective weight of slope (ω_e)		Units	Upstream	Downstream
Above the phreatic line	ω_{e1}	kN/m	116.91	167.04
Below the phreatic line	ω_{e2}		152.98	103.23
Through the fill and foundation	ω_{e3}		95.08	89.99
Total Effective weight	ω_e		364.97	360.26

Once the total effective weight of the upstream and downstream slopes were found, Table III.14, the total vertical effective force (σ_F) and effective shear stress (σ_v') acting on the individual slopes were calculated.

Upstream slope:

$$\sigma_{F_u} = \omega_{eu} = 364.97\ \text{kN/m}^2 \qquad \text{(III.9)}$$

$$\sigma_{vu}' = \frac{\sigma_{Fu} - u_{vu}}{b_u} = \frac{364.97 - 127.36}{9} = 26.40\ \text{kN/m}^2 \qquad \text{(III.10)}$$

Downstream slope:

$$\sigma_{F_d} = \omega_{ed} = 360.26\ \text{kN/m}^2 \qquad \text{(III.11)}$$

$$\sigma_{vd}' = \frac{\sigma_{Fd} - u_{vd}}{b_d} = \frac{360.26 - 96.10}{12} = 22.01\,kN/m^2 \qquad (III.12)$$

Table III.15 Active earth pressures from the core , upstream and downstream slopes

Active earth pressures (P_a)		Units	Upstream	Core	Downstream
Above the phreatic line	P_{a1}	kN per m length of dam	9.51	11.72	19.57
Below the phreatic line	P_{a2}		29.96	27.41	14.98
Through the fill and foundation	P_{a3}		17.52	18.17	14.96
Total active earth pressure	P_{aT}		56.99	57.30	49.51

Table III.16 Passive pressure: force acting on the slope from the embankment's foundation

Passive earth pressures (P_p)		Units	Upstream	Downstream
Effective earth pressure	σ_P'	kN/m^2	131.89	125.15
Horizontal passive earth pressure	σ_P		150.38	138.94
Passive earth pressure force	P_p	kN per m length of dam	37.60	34.74

III.2 Modified Slope Stability Model

Summary of results evaluated deterministically, in *Chapter 5: Subsection 5.6*, using the modified upstream and downstream slope stability models for the physical embankment model constructed of London Clay (LC).

III.2.1 Rainfall scenario: 70mm in 1hr

The calculated vertical and horizontal stresses, effective stresses, pore pressures and total active and passive earth pressure forces required to determine the factor of safety for the embankment's upstream and downstream slopes when constructed of London Clay are presented in Tables III.17 to III.27. For the applied active and passive earth pressure coefficients, see Eqns. (III.1 and III.2).

III.2.2 Rainfall scenario: prolonged rainfall over 24hrs (10mm/hr)

Here, Tables III.28 to III.35 show the calculated vertical and horizontal stresses, effective stresses, pore pressures and total active and passive earth pressure forces required to determine the factor of safety for the embankment's upstream and downstream slopes when constructed of London Clay.

Table III.17 Pore pressures acting through the upstream slope, core and downstream slope

Pore pressure (u)		Units	S_r = 56 %			S_r = 76 %		
			Upstream	Core	Downstream	Upstream	Core	Downstream
Above the phreatic line	u_{1a}	kN/m^2	0.19	0.06	0.25	0.97	0.31	1.27
	u_{1b}		0.19	0.06	0.25	0.97	0.31	1.27
Below the phreatic line	u_2		13.78	11.90	7.50	14.56	12.15	7.51
Through the fill and foundation	u_3		18.69	16.81	12.40	19.46	17.06	12.41
Pore pressure in the vertical direction	u_v		129.11		133.99	136.08		140.11

Table III.18 Vertical stresses acting on the upstream slope, core and downstream slope

Vertical stress (σ_v)		Units	S_r = 56 %			S_r = 76 %		
			Upstream	Core	Downstream	Upstream	Core	Downstream
Above the phreatic line	σ_{v1a}	kN/m^2	0.40	0.13	0.52	1.98	0.63	2.60
	σ_{v1b}		27.51	30.50	40.05	28.24	31.14	42.43
Below the phreatic line	σ_{v2}		55.33	29.08	48.55	56.06	59.92	50.98
Through the fill and foundation	σ_{v3}		65.38	66.98	55.37	66.11	67.87	57.88

Table III.19 Vertical effective stresses acting on the upstream slope, core and downstream slope

Vertical effective stress (σ_v')		Units	S_r = 56 %			S_r = 76 %		
			Upstream	Core	Downstream	Upstream	Core	Downstream
Above the phreatic line	σ_{v1a}'	kN/m^2	0.20	0.06	0.26	1.01	0.32	1.33
	σ_{v1b}'		27.32	30.44	39.80	27.28	30.83	41.17
Below the phreatic line	σ_{v2}'		41.55	47.18	32.55	41.51	47.77	34.93
Through the fill and foundation	σ_{v3}'		46.69	50.17	42.97	46.64	50.81	45.46

Table III.20 Horizontal effective stresses acting on the upstream slope, core and downstream slope

Horizontal effective stress (σ_h')		Units	S_r = 56 %			S_r = 76 %		
			Upstream	Core	Downstream	Upstream	Core	Downstream
Above the phreatic line	σ_{h1a}'	kN/m^2	-6.90	-6.97	-6.87	-6.50	-6.84	-6.35
	σ_{h1b}'		6.39	7.92	12.51	6.37	8.11	13.18
Below the phreatic line	σ_{h2}'		13.37	16.13	8.96	13.35	16.42	10.12
Through the fill and foundation	σ_{h3}'		15.89	17.59	14.06	15.87	17.91	15.29

Table III.21 Horizontal stresses acting on the upstream slope, core and downstream slope

Horizontal stress (σ_h)		Units	S_r = 56 %			S_r = 76 %		
			Upstream	Core	Downstream	Upstream	Core	Downstream
Above the phreatic line	σ_{h1a}	kN/m^2	7.10	7.03	7.12	7.47	7.15	7.62
	σ_{h1b}		6.59	7.98	12.76	7.34	8.42	14.45
Below the phreatic line	σ_{h2}		27.15	28.03	16.46	27.90	28.57	17.63
Through the fill and foundation	σ_{h3}		34.58	34.40	26.47	35.33	34.97	27.70

Table III.22 The effective weight of soil in the upstream and downstream slopes

Effective weight of slope (ω_e)		Units	S_r = 56 %		S_r = 76 %	
			Upstream	Downstream	Upstream	Downstream
Above the phreatic line	ω_{e1a}	kN/m	0.59	1.49	2.95	7.48
	ω_{e1b}		106.24	289.26	106.21	289.46
Below the phreatic line	ω_{e2}		145.03	9.86	145.03	9.93
Through the fill and foundation	ω_{e3}		90.38	81.82	90.38	82.79
Total Effective weight	ω_e		342.25	382.43	344.57	389.67

Table III.23 Total vertical effective force (σ_F) and effective shear stress (σ_v') acting on the upstream and downstream slopes

		Units	S_r = 56 %		S_r = 76 %	
			Upstream	Downstream	Upstream	Downstream
Total vertical effective force	σ_F	kN/m^2	342.25	382.43	344.57	389.67
Vertical effective shear stress	σ_v'		23.68	20.70	23.17	20.80

Table III.24 Active earth pressures from the core, upstream and downstream slopes

Active earth pressures (P_a)		Units	S_r = 56 %			S_r = 76 %		
			Upstream	Core	Downstream	Upstream	Core	Downstream
Above the phreatic line	P_{a1a}	kN per m length of dam	0.07	0.02	0.09	0.37	0.11	0.49
	P_{a1b}		10.91	13.41	22.74	11.23	13.72	23.38
Below the phreatic line	P_{a2}		23.37	21.74	11.57	24.41	22.33	12.09
Through the fill and foundation	P_{a3}		15.43	15.61	12.48	15.81	15.88	12.75
Total active earth pressure	P_{aT}		49.78	50.78	46.89	51.81	52.04	48.71

Table III.25 Passive pressure: force acting on the upstream and downstream slopes from the embankment's foundation

Passive earth pressures (P_a)		Units	S_r = 56 %		S_r = 76 %	
			Upstream	Downstream	Upstream	Downstream
Effective earth pressure	σ_P'	kN/m^2	109.51	101.92	109.42	107.01
Horizontal passive earth pressure	σ_P		128.20	114.32	128.88	119.42
Total passive earth pressure	P_{pT}	kN per m length of dam	32.05	28.58	32.22	29.86

Table III.26 Total resultant shearing force and horizontal driving force acting on the embankment's slopes

Passive earth pressures (P_a)		Units	S_r = 56 %		S_r = 76 %	
			Upstream	Downstream	Upstream	Downstream
Total effective shear stress	τ'	kN/m^2	13.62	12.54	13.43	12.57
Total horizontal driving force	H	kN per m length of dam	54.58	71.98	57.50	74.00
Resultant shearing force	R		122.58	150.42	120.88	150.83

Table III.27 Pore pressures acting through the upstream slope, core and downstream slope

Pore pressure (u)		Units	S_r = 56 %			S_r = 76 %		
			Upstream	Core	Downstream	Upstream	Core	Downstream
Above the phreatic line	u_{1a}	kN/m^2	0.95	0.30	1.25	2.99	1.00	3.99
	u_{1b}		0.95	0.30	1.25	2.99	1.00	3.99
Below the phreatic line	u_2		14.54	12.15	7.51	16.58	12.84	7.53
Through the fill and foundation	u_3		19.45	17.05	12.41	21.49	17.74	12.44
Pore pressure in the vertical direction	u_v		135.94		139.98	154.31		156.52

Table III.28 Vertical stresses acting on the upstream slope, core and downstream slope

Vertical stress (σ_v)		Units	S_r = 56 %			S_r = 76 %		
			Upstream	Core	Downstream	Upstream	Core	Downstream
Above the phreatic line	σ_{v1a}	kN/m^2	1.95	0.62	2.55	6.13	2.04	8.17
	σ_{v1b}		27.75	30.58	41.66	28.81	31.34	46.82
Below the phreatic line	σ_{v2}		55.57	59.16	50.17	56.63	60.11	55.40
Through the fill and foundation	σ_{v3}		65.61	67.05	56.99	66.68	68.06	62.30

Table III.29 Vertical effective stresses acting on the upstream slope, core and downstream slope

Vertical effective stress (σ_v')		Units	S_r = 56 %			S_r = 76 %		
			Upstream	Core	Downstream	Upstream	Core	Downstream
Above the phreatic line	σ_{v1a}'	kN/m^2	1.00	0.32	1.31	3.14	1.05	4.18
	σ_{v1b}'		26.80	30.27	4042	25.82	30.34	42.83
Below the phreatic line	σ_{v2}'		41.03	47.01	34.16	40.05	47.27	39.29
Through the fill and foundation	σ_{v3}'		46.17	50.00	44.58	45.19	50.31	49.86

Table III.30 Horizontal effective stresses acting on the upstream slope, core and downstream slope

Horizontal effective stress (σ_h')		Units	S_r = 56 %			S_r = 76 %		
			Upstream	Core	Downstream	Upstream	Core	Downstream
Above the phreatic line	σ_{h1a}'	kN/m^2	-6.51	-6.85	-6.36	-5.46	-6.49	-4.95
	σ_{h1b}'		6.14	7.84	12.81	5.66	7.87	14.00
Below the phreatic line	σ_{h2}'		13.12	16.05	9.74	12.63	16.18	12.26
Through the fill and foundation	σ_{h3}'		15.63	17.51	14.86	15.15	17.67	17.45

Table III.31 Horizontal stresses acting on the upstream slope, core and downstream slope

Horizontal stress (σ_h)		Units	S_r = 56 %			S_r = 76 %		
			Upstream	Core	Downstream	Upstream	Core	Downstream
Above the phreatic line	σ_{h1a}	kN/m^2	7.47	7.15	7.61	8.46	7.49	8.94
	σ_{h1b}		7.09	8.14	14.06	8.65	8.87	17.99
Below the phreatic line	σ_{h2}		27.66	28.19	17.25	29.22	29.02	19.79
Through the fill and foundation	σ_{h3}		35.08	34.56	27.27	36.64	35.41	29.88

Table III.32 The effective weight of soil in the upstream and downstream slopes

Effective weight of slope (ω_e)		Units	S_r = 56 %		S_r = 76 %	
			Upstream	Downstream	Upstream	Downstream
Above the phreatic line	ω_{e1a}	kN/m	2.90	7.36	8.97	23.56
	ω_{e1b}		104.28	284.22	101.01	275.40
Below the phreatic line	ω_{e2}		145.03	9.91	145.03	10.06
Through the fill and foundation	ω_{e3}		90.38	81.82	90.38	82.79
Total Effective weight	ω_e		342.60	383.31	345.40	391.81

Table III.33 Total vertical effective force (σ_F) and effective shear stress (σ_v') acting on the upstream and downstream slopes

		Units	S_r = 56 %		S_r = 76 %	
			Upstream	Downstream	Upstream	Downstream
Total vertical effective force	σ_F	kN/m^2	342.60	383.31	345.40	391.81
Vertical effective shear stress	σ_v'		22.96	20.28	21.23	19.61

Table III.34 Active earth pressures from the core, upstream and downstream slopes

Active earth pressures (P_a)		Units	S_r = 56 %			S_r = 76 %		
			Upstream	Core	Downstream	Upstream	Core	Downstream
Above the phreatic line	P_{a1a}	kN per metre length of dam	0.36	0.11	0.48	1.29	0.38	1.82
	P_{a1b}		11.05	13.47	23.00	11.20	13.83	23.38
Below the phreatic line	P_{a2}		24.06	21.93	11.85	26.23	22.87	12.84
Through the fill and foundation	P_{a3}		15.68	15.69	12.56	16.46	16.11	12.95
Total active earth pressure	P_{aT}		51.16	51.20	47.90	55.19	53.19	51.00

Table III.35 Passive pressure: force acting on the upstream and downstream slopes from the embankment's foundation

Passive earth pressure (P_a)		Units	S_r = 56 %		S_r = 76 %	
			Upstream	Downstream	Upstream	Downstream
Effective earth pressure	σ_P'	kN/m^2	108.45	105.21	106.45	115.99
Horizontal passive earth pressure	σ_P		127.89	117.62	127.94	128.42
Total passive earth pressure	P_{pT}	kN per m length of dam	31.97	29.41	31.98	32.11

Table III.36 Total resultant shearing force and horizontal driving force acting on the embankment's slopes

Passive earth pressures (P_a)		Units	S_r = 56 %		S_r = 76 %	
			Upstream	Downstream	Upstream	Downstream
Total effective shear stress	τ'	kN/m^2	13.36	12.38	12.73	12.14
Total horizontal driving force	H	kN per m length of dam	56.09	72.96	61.16	76.27
Resultant shearing force	R		120.22	148.56	114.55	145.64

APPENDIX IV : THEORY OF PROBABILITY

This appendix summarises the theory relating to probability and the probability distribution models, focusing on the normal and lognormal distributions implemented in the reliability analysis. This appendix is an addition to *Chapter 3*.

IV.1 Numerical Measure of Probability

Probability can be expressed as a numerical measure that can be shown graphically using probability distribution. It compares the likelihood that an event can, and will, occur comparative to an event that will not occur. The numerical measure of probability can be derived from a set of axioms, which are the basis to the mathematics of probability (Hartford & Baecher, 2004). These axioms can only state what the properties of the probability are and not what the probability is. According to the axioms, the probability calculated is a function that assigns real numbers to events in a sample space. There are three fundamental axioms and can be stated as (Baecher & Christian, 2003):

Axiom 1: The probability P[E] of event (E) is a real non negative number and has a value between 0 and 1: $0 \le P\|E\| \le 1$

Axiom 2: The probability of an expected event (C) is P(C) = 1. Therefore, the sum of all possible probabilities of each individual event, E_i, is also equal to 1: $\sum_i P(E_i) = 1$

Axiom 3: The probability that either one or both events E_1 and E_2, can occur: $P(E_1 \cup E_2) = P(E_1) + P(E_2) - P(E_1 \cap E_2)$

For two mutually exclusive events, $P(E1 \cup E2)$, their union is equivalent to the summation of their individual probabilities:

$$P(E_1 \cup E_2) = P(E_1) + P(E_2) \quad \text{(IV.1)}$$

From the second axiom, it is possible to attain an equation to calculate the probability of failure as well as the risk and reliability. Since event (E) and its complement ($\overline{E}$), which is the event that E does not occur, are mutually exclusive then P(C) can be derived as:

$$P(C) = P(E_1 \cup \overline{E}) = P(E_1) + P(\overline{E}) = 1 \quad \text{(IV.2)}$$

$$P(\overline{E}) = 1 - P(E) \quad \text{(IV.3)}$$

IV.1.1 Random variables

Uncertain parameters, such as the physical characteristics of an embankment and its fill properties can be treated as random variables when carrying out a probabilistic analysis. A random variable is seen as a quantity where its magnitude is not a fixed value. This means that the assumed quantity can have any given number of values within a domain. The random variables are divided into, discrete and continuous random variables.

IV.1.2 Discrete random variables

Discrete random variables can only have specific isolated values, which mean their relative frequency of occurrence can only be calculated at those given points (Thoft-Christensen & Baker, 1982). Therefore, for a random variable (X) of a given sample area (S) the discrete values are denoted by $p_X(x)$, and is identified as the probability mass function (PMF) (Hartford & Baecher, 2004):

$$P_x(x) = P(X = x) \quad \text{(IV.4)}$$

For discrete random variables, the cumulative distribution is identified as the cumulative mass function (CMF) and satisfies the probability mass function, denoted by $p_X(x)$.

PMF is very similar to the probability density function (PDF), $f_X(x)$, but it is not a continuous function (Haldar & Mahadevan, 2000).

$$f_x(x) = P(X \le x) \tag{IV.5}$$

The cumulative distribution function (CDF) is calculated by summing up the PMFs to obtain $F_x(x)$ (Thoft-Christensen & Baker, 1982). Therefore, Eqn. (IV.5) can be rewritten in the form:

$$F_x(x) = P(X \le x) = \sum_{x_i \le x} p_x(x_i) \tag{IV.6}$$

where: $F_x(x)$ = Probability distribution function; p_x = Probability mass function.

IV.1.3 Continuous random variables

For continuous random variables, the CDF also describes the probability that a random variable (x) will take for a given value less than or equal to x (Baecher & Christian, 2003)**.** Thus, for the PDF of the random variable at known points along the x-axis, the differential form can be derived. Therefore, the PDF is the first derivative of the CDF and is expressed by Eqn. (IV.7). Figure IV.1 shows the probability density function and cumulative density function for a continuous random variable.

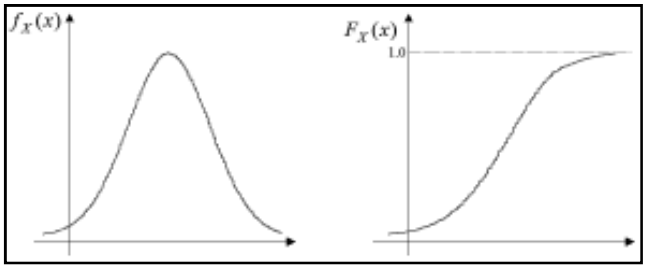

Figure IV.1 Probability density function, $f_X(x)$ and cumulative distribution function $F_X(x)$

$$f_x(x) = \frac{dF_x(x)}{dx} \tag{IV.7}$$

Any function that satisfies the following statements, Eqns. (IV.8 to IV.12), is classified as possible CDFs (Hartford & Baecher, 2004). The cumulative distribution function (CDF) can also be represented graphically, as shown in Figure IV.2.

$$F_X(-\infty) = 0 \qquad F_X(x) \ge 0 \tag{IV.8}$$

$$F_X(+\infty) = 1 \qquad f_X(x) \ge 0 \tag{IV.9}$$

which means:

$$F_X(x_0) = \int_{-\infty}^{x_0} f_x(x)dx \tag{IV.10}$$

$$F_X(+\infty) = \int_{-\infty}^{+\infty} f_X(x)dx = 1 \tag{IV.11}$$

Hence:

$$P(x_1 < X \leq x_2) = \int_{x_2}^{x_1} f_X(x)dx \tag{IV.12}$$

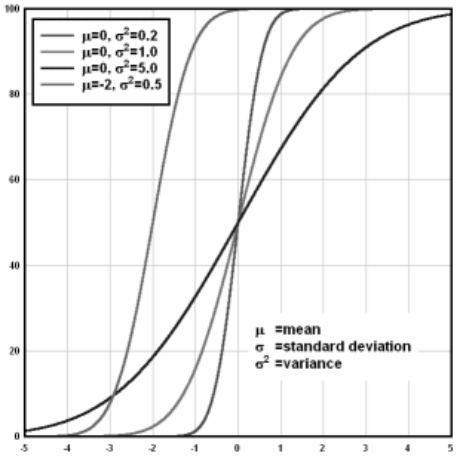

Figure IV.2 Cumulative distribution function

IV.1.4 Moments of random variables

The probability distributions can be characterised by their moments and expressed as F_X (Baecher & Christian, 2003). For a random variable, its first moment is evaluated as the weighted average of all the different values that the random variable can have. It is expressed as the mean (μ_X), or the expected value E(X), and is the first central moment of the area of the PDF (Abramson et al., 2002) and is expressed as:

$$Mean = E(X) = \mu_X = \frac{1}{n}\sum_{i=1}^{n} x_i \qquad \text{for discrete functions} \tag{IV.13}$$

$$E(X) = \mu_X \int_{-\infty}^{\infty} xf(x)dx \qquad \text{for continuous functions} \tag{IV.14}$$

The second moment of the random variable, relates to its variance, standard deviation and coefficient of variation (Griffiths, Fenton & Tveten, 2005). The variance, Var(X), is known as the second central moment and measures the amount of randomness about the mean (Abramson et al., 2002). This can then be expressed using Eqns. (IV.15 and IV.16).

Discrete functions: $$Var(X) = E(x_i - \mu_X)^2 = \frac{1}{n-1}\sum_{i=1}^{n}(x_i - \mu_X)^2 \quad \text{(IV.15)}$$

Continuous functions: $$E(x_i - \mu_X)^2 = \int_{-\infty}^{\infty}(x_i - \mu_X)^2 f(x)dx \quad \text{(IV.16)}$$

Once the variance is found, the standard deviation (σ_X), Eqn. (IV.17), of the random variable can be obtained. The coefficient of variance (COV) is therefore obtained by taking the ratio of the standard deviation and the mean to get a non-dimensional value, Eqn. (IV.18). As the value of the COV decreases, the uncertainty within the random variable also decreases or as COV increases the greater the uncertainty within the variable.

$$\sigma_x = \sqrt{\mathrm{Var(x)}} \quad \text{(IV.17)}$$

$$\mathrm{COV}(x) = \delta_x = \frac{\sigma_x}{\mu_x} \quad \text{(IV.18)}$$

IV.2 Common Probability Distribution Models

There are many probability distributions, but for structural applications the following distributions are important.

- Normal distribution
- Lognormal distribution
- Beta distribution
- Extreme value distribution

The beta distribution is a useful distribution to use as it arises from physical considerations and therefore can be applied to observed data (Hoek, 2007). The main advantage of this form of distribution is its flexibility and it can be applied to a random variable when it is known to be bounded by two limits. The other commonly used probability distribution mode is the extreme value distribution. This has a wide range of uses when solving engineering problems probabilistically. There are three forms of asymptotic extreme value distributions defined by Haldar and Mahadevan (2000) as:

- Type I, Gumbel-type distribution
- Type II, Fréchet-type distribution
- Type III, Weibull-type distribution

Only Type I and Type II distributions can be applied to probabilistic models that incorporate environmental phenomena. For this particular research project, beta and extreme value distributions are not considered and so only normal and lognormal distributions are consider here. These are summarised in the following subsections.

IV.2.1 Normal (Gaussian) distribution

The normal or Gaussian distribution, $N(\mu,\sigma)$, is the most common type of probability distribution function used, as many normal random variables conform to this type of distribution (Haldar & Mahadevan, 2000). This is more commonly used for probabilistic analyses in engineering, such as in geotechnical and structural engineering. When carrying out engineering problems, it provides a clear distribution that appears repeatedly as a limiting case of other probability distributions (Baecher & Christian, 2003). When defining a normal distribution, the true mean and true standard deviation of the values for the governing parameters have to be estimated (Hoek, 2007). Hence, the standard deviation and mean are the only parameters required for this particular distribution. Therefore, the probability density function, $f_x(x)$, and the cumulative distribution function, CDF, can be calculated using Eqns. (IV.19 and IV.20).

$$f_x(x) = \frac{1}{\sigma_x\sqrt{2\pi}} \exp\left[-\frac{1}{2}\left(\frac{x-\mu_x}{\sigma_x}\right)^2\right] \qquad -\infty < x < +\infty \qquad \text{(IV.19)}$$

$$P(X \le x) = F_x(x) = \int_{-\infty}^{x} \frac{1}{\sigma_x\sqrt{2\pi}} \exp\left[-\frac{1}{2}\left(\frac{x-\mu_x}{\sigma_x}\right)^2\right] dx \qquad \text{(IV.20)}$$

For certain applications the random variable (X) has to be transformed into a standard normal variable that has a mean of zero and a unit standard deviation (S), Eqn. (IV.21) (Haldar & Mahadevan, 2000).

$$\text{Unit standard deviation } = S = \frac{X-\mu_x}{\sigma_x} \qquad \text{(IV.21)}$$

Its related PDF and the corresponding CDF of S are therefore expressed using the following equations, Eqns. (IV.22 and IV.23).

$$f_S(S) = \frac{1}{\sqrt{2\pi}} \exp\left[-\frac{1}{2}S^2\right] \qquad -\infty < x < +\infty \qquad \text{(IV.22)}$$

$$\Phi(S) = F_S(S) = \int_{-\infty}^{S} \frac{1}{\sqrt{2\pi}} \exp\left[-\frac{1}{2}S^2\right] ds \qquad \text{(IV.23)}$$

All normal distributions are symmetrical, so when plotted graphically produce bell-shaped density curves with a single peak. Figure IV.3 shows an example of the different PDF curves produced using the Gaussian distribution. When carrying out the analysis, the shape and height of the normal density curve visibly changes depending on the standard deviation and mean values implemented. The mean value indicates where the peak of the density curve will occur and the standard deviation value defines the distribution of the bell-shaped curve (Haldar & Mahadevan, 2000). The corresponding CDFs of the normal distribution curves are shown in Figure IV.2.

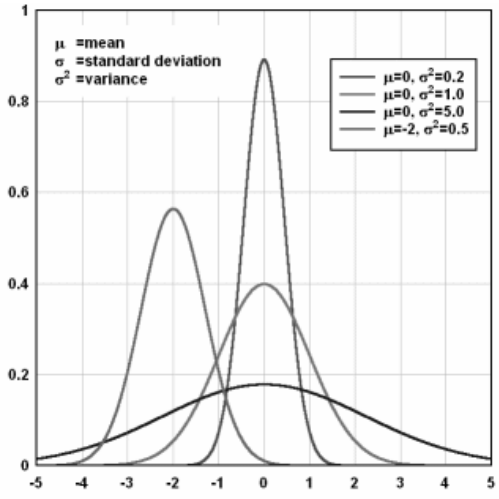

Figure IV.3. Probability density function for normal (Gaussian) distributions

IV.2.2 Lognormal distribution

The lognormal distribution, $LN(\lambda,\zeta)$, is based on the normal distribution of any random variable where its natural logarithm, log(X), is normally distributed (Haldar & Mahadevan, 2000). This means that the random variable cannot have a negative value, as its natural logarithm automatically removes any possibility of a negative value (Thoft-Christensen & Baker, 1982). This is extremely useful in engineering models as their parameters can never have negative values. The general expression for the PDF of the lognormal distribution can be equated, Eqn. (IV.24), where ζ_X and λ_X are the two parameters of the lognormal distribution.

$$f_X(x) = \frac{1}{\sqrt{2\pi}\zeta_X x} exp\left[-\frac{1}{2}\left(\frac{lnx - \lambda_X}{\zeta_X}\right)^2\right] \qquad 0 \le x < \infty \qquad \text{(IV.24)}$$

The PDF for the lognormal distribution is unsymmetrical. This means that its mean values will be different (Haldar & Mahadevan, 2000). Eqn. (IV.25) defines the CDF of the lognormal distribution, where Φ is the standard normal distribution function.

$$F_x(x) = \int_{-\infty}^{u} f_x(u)du = \Phi\left[\frac{\ln x - \lambda_X}{\zeta_X}\right] \tag{IV.25}$$

For the normal distribution, the following parameters λ and ζ^2 are expressed as:

$$\lambda_X = E(\ln X) = \ln \mu_X = \mu_{\ln X}$$

$$\zeta^2 = \mathrm{var}(\ln X) = \ln\left[1 + \left(\frac{\sigma_X}{\mu_X}\right)^2\right] = \ln(1 + \delta_X^2) = \sigma_{\ln X}^2$$

The lognormal random variable has a value between two limits (x_1 and x_2) its probability distribution can be obtained using the following equation (Haldar & Mahadevan, 2000), where its standard variable (S) is defined by Eqn. (IV.27). Therefore, Eqn. (IV.27) can be simplified and defined by Eqn. (IV.28).

$$P(a < X \le b) = \frac{1}{\sqrt{2\pi}} \int_{\frac{\ln b - \lambda_X}{\zeta_X}}^{\frac{\ln a - \lambda_X}{\zeta_X}} \exp\left[-\frac{1}{2}S^2\right] ds \tag{IV.26}$$

$$S = \frac{\ln X - \lambda_X}{\zeta_X} \tag{IV.27}$$

$$P(a < X \le b) = \Phi\left(\frac{\ln b - \lambda_X}{\zeta_X}\right) - \Phi\left(\frac{\ln a - \lambda_X}{\zeta_X}\right) \tag{IV.28}$$

APPENDIX V : RELY ROUTINE

This appendix provides a detailed outline about the Rely routine used to develop the probabilistic slope stability model (PSSM) and the advanced probabilistic slope stability model with precipitation effects (APSMP). The Rely routine (Rely.For) is a structural reliability analysis routine based on advanced first order second moment theory (FOSM) and determines the failure probability and reliability index of any structure under investigation (Ramachandran & Baker 1982). The routine was written using FORTRAN code, and was compiled in 1982 by the Department of Civil Engineering at Imperial College. For the Rely routine GFUNC (Q, X, MF, IR), which defines the structure's failure function, $g(x_i) = g(x_1, x_2, \dots\dots, x_n)$, has to be developed. The GFUNC subroutine can contain an infinite number of statements, $M = g(x_i)$, where M is the safety margin. These individual statements can have calls to other subroutines, either within the subroutine itself or to a separate file. Once all the relevant statements are defined within the routine a final statement, $M = f(Y)$, is written at the end of the subroutine, where $Y=f(x)$.

It is imperative that the random variables are identified as either stochastic or deterministic. The Rely routine also recognises the different probability distributions:

- Normal distribution
- Lognormal distributions
- Extreme Value Type I and Type II distributions

Other probability distributions can be incorporated into the routine by simply adding the appropriate subroutines to the main Rely routine.

Here, the standard Rackwitz-Fiessler iterative approach is implemented to determine the most probable failure point of the limit state function within the domain of the routine. The compiled results obtained for each failure mode include the reliability index (β), failure probability (P_f), and residual value for the individual failure modes.

APPENDIX VI : PARAMETER CODES AND FITTING PARAMETERS FOR THE SELECTED SOIL MODELS

VI.1 Parameter Codes for Soil Models M1 to M7

M1: Alluvial Soil

MODEL	H_w	S_r	EMBANKMENT GEOMETRIES (SG)				
M1	R1 (H_w = 1.0m)	58.63 - 95.26 %	Upstream / Downstream	1 : 2.5	1 : 3.0	1 : 3.5	1 : 4.0
			1 : 2.5	M1R1SG1	M1R1SG2	M1R1SG3	M1R1SG4
			1 : 3.0		M1R1SG5	M1R1SG6	M1R1SG7
			1 : 3.5		M1R1SG8	M1R1SG9	M1R1SG10
			1 : 4.0		M1R1SG11	M1R1SG12	M1R1SG13
	R2 (H_w = 1.5m)	58.63 - 95.26 %	Upstream / Downstream	1 : 2.5	1 : 3.0	1 : 3.5	1 : 4.0
			1 : 2.5	M1R2SG1	M1R2SG2	M1R2SG3	M1R2SG4
			1 : 3.0		M1R2SG5	M1R2SG6	M1R2SG7
			1 : 3.5		M1R2SG8	M1R2SG9	M1R2SG10
			1 : 4.0		M1R2SG11	M1R2SG12	M1R2SG13
	R3 (H_w = 2.0m)	58.63 - 95.26 %	Upstream / Downstream	1 : 2.5	1 : 3.0	1 : 3.5	1 : 4.0
			1 : 2.5	M1R3SG1	M1R3SG2	M1R3SG3	M1R3SG4
			1 : 3.0		M1R3SG5	M1R3SG6	M1R3SG7
			1 : 3.5		M1R3SG8	M1R3SG9	M1R3SG10
			1 : 4.0		M1R3SG11	M1R3SG12	M1R3SG13

M2: Moist Clay (Silty Clay)

MODEL	H_w	S_r	EMBANKMENT GEOMETRIES (SG)				
M2	R1 (H_w = 1.0m)	58.63 - 95.26 %	Upstream / Downstream	1 : 2.5	1 : 3.0	1 : 3.5	1 : 4.0
			1 : 2.5	M2R1SG1	M2R1SG2	M2R1SG3	M2R1SG4
			1 : 3.0		M2R1SG5	M2R1SG6	M2R1SG7
			1 : 3.5		M2R1SG8	M2R1SG9	M2R1SG10
			1 : 4.0		M2R1SG11	M2R1SG12	M2R1SG13
	R2 (H_w = 1.5m)	58.63 - 95.26 %	Upstream / Downstream	1 : 2.5	1 : 3.0	1 : 3.5	1 : 4.0
			1 : 2.5	M2R2SG1	M2R2SG2	M2R2SG3	M2R2SG4
			1 : 3.0		M2R2SG5	M2R2SG6	M2R2SG7
			1 : 3.5		M2R2SG8	M2R2SG9	M2R2SG10
			1 : 4.0		M2R2SG11	M2R2SG12	M2R2SG13
	R3 (H_w = 2.0m)	58.63 - 95.26 %	Upstream / Downstream	1 : 2.5	1 : 3.0	1 : 3.5	1 : 4.0
			1 : 2.5	M2R3SG1	M2R3SG2	M2R3SG3	M2R3SG4
			1 : 3.0		M2R3SG5	M2R3SG6	M2R3SG7
			1 : 3.5		M2R3SG8	M2R3SG9	M2R3SG10
			1 : 4.0		M2R3SG11	M2R3SG12	M2R3SG13

M3A: London Clay

MODEL	H_w	S_r	EMBANKMENT GEOMETRIES (SG)				
M3A	R1 (H_w=1.0m)	58.63 - 95.26 %	Upstream / Downstream	1 : 2.5	1 : 3.0	1 : 3.5	1 : 4.0
			1 : 2.5	M3AR1SG1	M3AR1SG2	M3AR1SG3	M3AR1SG4
			1 : 3.0		M3AR1SG5	M3AR1SG6	M3AR1SG7
			1 : 3.5		M3AR1SG8	M3AR1SG9	M3AR1SG10
			1 : 4.0		M3AR1SG11	M3AR1SG12	M3AR1SG13
	R2 (H_w=1.5m)	58.63 - 95.26 %	Upstream / Downstream	1 : 2.5	1 : 3.0	1 : 3.5	1 : 4.0
			1 : 2.5	M3AR2SG1	M3AR2SG2	M3AR2SG3	M3AR2SG4
			1 : 3.0		M3AR2SG5	M3AR2SG6	M3AR2SG7
			1 : 3.5		M3AR2SG8	M3AR2SG9	M3AR2SG10
			1 : 4.0		M3AR2SG11	M3AR2SG12	M3AR2SG13
	R3 (H_w=2.0m)	58.63 - 95.26 %	Upstream / Downstream	1 : 2.5	1 : 3.0	1 : 3.5	1 : 4.0
			1 : 2.5	M3AR3SG1	M3AR3SG2	M3AR3SG3	M3AR3SG4
			1 : 3.0		M3AR3SG5	M3AR3SG6	M3AR3SG7
			1 : 3.5		M3AR3SG8	M3AR3SG9	M3AR3SG10
			1 : 4.0		M3AR3SG11	M3AR3SG12	M3AR3SG13

M3B: London Clay

MODEL	H_w	S_r	EMBANKMENT GEOMETRIES (SG)				
M3B	R1 (H_w= 1.0m)	58.63 - 95.26 %	Upstream / Downstream	1 : 2.5	1 : 3.0	1 : 3.5	1 : 4.0
			1 : 2.5	M3BR1SG1	M3BR1SG2	M3BR1SG3	M3BR1SG4
			1 : 3.0		M3BR1SG5	M3BR1SG6	M3BR1SG7
			1 : 3.5		M3BR1SG8	M3BR1SG9	M3BR1SG10
			1 : 4.0		M3BR1SG11	M3BR1SG12	M3BR1SG13
	R2 (H_w = 1.5m)	58.63 - 95.26 %	Upstream / Downstream	1 : 2.5	1 : 3.0	1 : 3.5	1 : 4.0
			1 : 2.5	M3BR2SG1	M3BR2SG2	M3BR2SG3	M3BR2SG4
			1 : 3.0		M3BR2SG5	M3BR2SG6	M3BR2SG7
			1 : 3.5		M3BR2SG8	M3BR2SG9	M3BR2SG10
			1 : 4.0		M3BR2SG11	M3BR2SG12	M3BR2SG13
	R3 (H_w = 2.0m)	58.63 - 95.26 %	Upstream / Downstream	1 : 2.5	1 : 3.0	1 : 3.5	1 : 4.0
			1 : 2.5	M3BR3SG1	M3BR3SG2	M3BR3SG3	M3BR3SG4
			1 : 3.0		M3BR3SG5	M3BR3SG6	M3BR3SG7
			1 : 3.5		M3BR3SG8	M3BR3SG9	M3BR3SG10
			1 : 4.0		M3BR3SG11	M3BR3SG12	M3BR3SG13

M4: Lower Oxford Clay

MODEL	H_w	S_r	EMBANKMENT GEOMETRIES (SG)				
M4	R1 (H_w = 1.0m)	58.63 - 95.26 %	Upstream / Downstream	1 : 2.5	1 : 3.0	1 : 3.5	1 : 4.0
			1 : 2.5	M4R1SG1	M4R1SG2	M4R1SG3	M4R1SG4
			1 : 3.0		M4R1SG5	M4R1SG6	M4R1SG7
			1 : 3.5		M4R1SG8	M4R1SG9	M4R1SG10
			1 : 4.0		M4R1SG11	M4R1SG12	M4R1SG13
	R2 (H_w = 1.5m)	58.63 - 95.26 %	Upstream / Downstream	1 : 2.5	1 : 3.0	1 : 3.5	1 : 4.0
			1 : 2.5	M4R2SG1	M4R2SG2	M4R2SG3	M4R2SG4
			1 : 3.0		M4R2SG5	M4R2SG6	M4R2SG7
			1 : 3.5		M4R2SG8	M4R2SG9	M4R2SG10
			1 : 4.0		M4R2SG11	M4R2SG12	M4R2SG13
	R3 (H_w = 2.0m)	58.63 - 95.26 %	Upstream / Downstream	1 : 2.5	1 : 3.0	1 : 3.5	1 : 4.0
			1 : 2.5	M4R3SG1	M4R3SG2	M4R3SG3	M4R3SG4
			1 : 3.0		M4R3SG5	M4R3SG6	M4R3SG7
			1 : 3.5		M4R3SG8	M4R3SG9	M4R3SG10
			1 : 4.0		M4R3SG11	M4R3SG12	M4R3SG13

M5: Gault Clay

MODEL	H_w	S_r	EMBANKMENT GEOMETRIES (SG)				
M5	R1 (H_w = 1.0m)	58.63 - 95.26 %	Upstream / Downstream	1 : 2.5	1 : 3.0	1 : 3.5	1 : 4.0
			1 : 2.5	M5R1SG1	M5R1SG2	M5R1SG3	M5R1SG4
			1 : 3.0		M5R1SG5	M5R1SG6	M5R1SG7
			1 : 3.5		M5R1SG8	M5R1SG9	M5R1SG10
			1 : 4.0		M5R1SG11	M5R1SG12	M5R1SG13
	R2 (H_w = 1.5m)	58.63 - 95.26 %	Upstream / Downstream	1 : 2.5	1 : 3.0	1 : 3.5	1 : 4.0
			1 : 2.5	M5R2SG1	M5R2SG2	M5R2SG3	M5R2SG4
			1 : 3.0		M5R2SG5	M5R2SG6	M5R2SG7
			1 : 3.5		M5R2SG8	M5R2SG9	M5R2SG10
			1 : 4.0		M5R2SG11	M5R2SG12	M5R2SG13
	R3 (H_w = 2.0m)	58.63 - 95.26 %	Upstream / Downstream	1 : 2.5	1 : 3.0	1 : 3.5	1 : 4.0
			1 : 2.5	M5R3SG1	M5R3SG2	M5R3SG3	M5R3SG4
			1 : 3.0		M5R3SG5	M5R3SG6	M5R3SG7
			1 : 3.5		M5R3SG8	M5R3SG9	M5R3SG10
			1 : 4.0		M5R3SG11	M5R3SG12	M5R3SG13

M6: Silty Gravely Clay

MODEL	H_w	S_r	EMBANKMENT GEOMETRIES (SG)				
M6	R1 (H_w = 1.0m)	58.63 - 95.26 %	Upstream / Downstream	1 : 2.5	1 : 3.0	1 : 3.5	1 : 4.0
			1 : 2.5	M6R1SG1	M6R1SG2	M6R1SG3	M6R1SG4
			1 : 3.0		M6R1SG5	M6R1SG6	M6R1SG7
			1 : 3.5		M6R1SG8	M6R1SG9	M6R1SG10
			1 : 4.0		M6R1SG11	M6R1SG12	M6R1SG13
	R2 (H_w = 1.5m)	58.63 - 95.26 %	Upstream / Downstream	1 : 2.5	1 : 3.0	1 : 3.5	1 : 4.0
			1 : 2.5	M6R2SG1	M6R2SG2	M6R2SG3	M6R2SG4
			1 : 3.0		M6R2SG5	M6R2SG6	M6R2SG7
			1 : 3.5		M6R2SG8	M6R2SG9	M6R2SG10
			1 : 4.0		M6R2SG11	M6R2SG12	M6R2SG13
	R3 (H_w = 2.0m)	58.63 - 95.26 %	Upstream / Downstream	1 : 2.5	1 : 3.0	1 : 3.5	1 : 4.0
			1 : 2.5	M6R3SG1	M6R3SG2	M6R3SG3	M6R3SG4
			1 : 3.0		M6R3SG5	M6R3SG6	M6R3SG7
			1 : 3.5		M6R3SG8	M6R3SG9	M6R3SG10
			1 : 4.0		M6R3SG11	M6R3SG12	M6R3SG13

M7: Medium Silt

MODEL	H_w	S_r	EMBANKMENT GEOMETRIES (SG)				
M7	R1 (H_w = 1.0m)	58.63 - 95.26 %	Upstream / Downstream	1 : 2.5	1 : 3.0	1 : 3.5	1 : 4.0
			1 : 2.5	M7R1SG1	M7R1SG2	M7R1SG3	M7R1SG4
			1 : 3.0		M7R1SG5	M7R1SG6	M7R1SG7
			1 : 3.5		M7R1SG8	M7R1SG9	M7R1SG10
			1 : 4.0		M7R1SG11	M7R1SG12	M7R1SG13
	R2 (H_w = 1.5m)	58.63 - 95.26 %	Upstream / Downstream	1 : 2.5	1 : 3.0	1 : 3.5	1 : 4.0
			1 : 2.5	M7R2SG1	M7R2SG2	M7R2SG3	M7R2SG4
			1 : 3.0		M7R2SG5	M7R2SG6	M7R2SG7
			1 : 3.5		M7R2SG8	M7R2SG9	M7R2SG10
			1 : 4.0		M7R2SG11	M7R2SG12	M7R2SG13
	R3 (H_w = 2.0m)	58.63 - 95.26 %	Upstream / Downstream	1 : 2.5	1 : 3.0	1 : 3.5	1 : 4.0
			1 : 2.5	M7R3SG1	M7R3SG2	M7R3SG3	M7R3SG4
			1 : 3.0		M7R3SG5	M7R3SG6	M7R3SG7
			1 : 3.5		M7R3SG8	M7R3SG9	M7R3SG10
			1 : 4.0		M7R3SG11	M7R3SG12	M7R3SG13

VI.2 Fitting Parameters for Specific Soil Types

Soil water retention, hydraulic conductivity and fitting parameters relating to specific soils, identified by Rawls, Brakensiek and Saxton (1982), Table VI.1, and Carsel and Parrish (1988), Table VI.2.

Table VI.1 Average values for selected soil water retention and hydraulic conductivity parameters for 11 major soil textural groups according to Rawls, Brakensiek and Saxton (1982)

Texture	θ_r	θ_s	α l/cm	n	K_s cm/d
Sand	0.020	**0.417**	**0.138**	**1.592**	**504.0**
Loamy sand	**0.035**	**0.401**	**0.115**	**1.474**	**146.6**
Sandy loam	**0.041**	**0.412**	**0.068**	**1.322**	**62.16**
Loam	**0.027**	**0.434**	**0.090**	**1.220**	**16.32**
silt loam	**0.015**	**0.486**	**0.048**	**1.211**	**31.68**
Sandy clay loam	**0.068**	**0.330**	**0.036**	**1.250**	**10.32**
Clay loam	**0.075**	**0.390**	**0.039**	**1.194**	**5.52**
Silty clay loam	**0.040**	**0.432**	**0.031**	**1.151**	**3.60**
Sandy clay	**0.109**	**0.321**	**0.034**	**1.168**	**2.88**
Silty clay	**0.056**	**0.423**	**0.029**	**1.127**	**2.16**
Clay	**0.090**	**0.385**	**0.027**	**1.131**	**1.44**

Table VI.2 Average values for selected soil water retention and hydraulic conductivity parameters for 12 major soil textural groups according to Carsel and Parrish (1988)

Texture	θ_r	θ_s	α l/cm	n	K_s cm/d
Sand	**0.045**	0.43	0.145	2.68	712.8
Loamy Sand	0.057	0.41	0.124	2.28	350.2
Sandy Loam	0.065	0.41	0.075	1.89	106.1
Loam	0.078	0.43	0.036	1.56	24.96
silt	0.034	0.46	0.016	1.37	6.00
silt Loam	0.067	0.45	0.020	1.41	10.80
Sandy Clay Loam	0.100	0.39	0.059	1.48	31.44
Clay Loam	0.0%	0.41	0.019	1.31	6.24
Silty Clay Loam	0.089	0.43	0.010	1.23	1.68
Sandy Clay	0.100	0.38	0.027	1.23	2.88
Silty Clay	0.070	0.36	0.005	1.09	0.48
Clay	0.068	0.38	0.008	1.09	4.80

APPENDIX VII : RESULTS - PROBABILISTIC SLOPE STABILITY ANALYSIS (NO RAINFALL)

Tables VII.1 to VII.6 show the complete set of reliability indices (β_{up} and β_{dwn}) collated for upstream (FM1) and downstream (FM2) failure for all soil models (M1 to M7) when implementing the probabilistic slope stability model (PSSM), subjected to:

- A range of slope configurations (SG1 to SG13).
- Headwater height scenarios R1 (H_w = 1.0m), R2 (H_w = 1.5m) and R3 (H_w = 2.0m).
- Similar degrees of saturation (S_r = 56 - 59.4 %, 72.0 - 76.5 % and 86.5 - 89.8 %).

Table VII.1 Reliability indices for FM1 and FM2 for SG1 to SG7 for M1 to M7 with varying degrees of saturation when H_w = 1.0m

S_r	Model	Reliability Index (β) when H_w = 1.0 m													
		SG1		SG2		SG3		SG4		SG5		SG6		SG7	
		FM1	FM2	FM1	FM2	FM1	FM2	FM1	FM2	FM1	FM2	FM1	FM2	FM1	FM2
%		β_{up}	β_{dwn}	β_{up}	β_{dwn}	β_{up}	β_{dwn}	β_{up}	β_{dwn}	β_{up}	β_{dwn}	β_{up}	β_{dwn}	β_{up}	β_{dwn}
56.0 - 59.4	M1	2.44	1.97	2.69	1.99	2.90	2.00	3.07	2.02	2.68	2.23	2.89	2.24	3.07	2.25
	M2	3.80	3.16	4.20	3.18	4.53	3.20	4.80	3.22	4.19	3.54	4.52	3.56	4.79	3.58
	M3A	3.43	2.69	3.97	2.72	4.43	2.74	4.82	2.76	3.96	3.23	4.41	3.25	4.80	3.27
	M3B	3.04	2.09	3.64	2.12	4.15	2.15	4.58	2.18	3.63	2.70	4.13	2.73	4.56	2.75
	M4	4.76	4.07	5.12	4.09	5.42	4.11	5.66	4.13	5.10	4.41	5.40	4.43	5.64	4.45
	M5	4.36	3.73	4.83	3.92	5.07	3.94	5.26	3.95	4.64	4.00	4.88	4.02	5.08	4.04
	M6	3.84	3.34	4.11	3.36	4.33	3.37	4.51	3.39	4.09	3.59	4.31	3.60	4.50	3.62
	M7	1.54	0.76	1.96	0.79	2.32	0.82	2.62	0.84	1.94	1.19	2.30	1.21	2.61	1.24
72.0 - 76.5	M1	2.43	1.97	2.68	1.99	2.89	2.00	3.06	2.02	2.67	2.23	2.88	2.24	3.06	2.25
	M2	3.79	3.16	4.20	3.18	4.53	3.20	4.80	3.22	4.18	3.54	4.51	3.56	4.78	3.58
	M3A	3.40	2.68	3.95	2.71	4.41	2.73	4.80	2.75	3.94	3.22	4.40	3.24	4.78	3.26
	M3B	3.00	2.08	3.60	2.11	4.11	2.13	4.54	2.16	3.59	2.68	4.10	2.71	4.53	2.73
	M4	4.75	4.07	5.12	4.09	5.41	4.11	5.66	4.13	5.10	4.41	5.40	4.43	5.64	4.45
	M5	4.36	3.74	4.83	3.92	5.07	3.94	5.26	3.96	4.64	4.01	4.88	4.03	5.08	4.05
	M6	3.83	3.34	4.10	3.36	4.33	3.37	4.51	3.39	4.09	3.59	4.31	3.61	4.50	3.62
	M7	1.53	0.77	1.95	0.80	2.31	0.82	2.61	0.85	1.94	1.19	2.29	1.22	2.60	1.24
86.5 - 89.8	M1	2.42	1.97	2.67	1.99	2.88	2.00	3.05	2.02	2.66	2.23	2.87	2.24	3.05	2.25
	M2	3.78	3.16	4.19	3.18	4.52	3.20	4.80	3.22	4.17	3.54	4.50	3.56	4.78	3.58
	M3A	3.38	2.67	3.94	2.70	4.40	2.73	4.79	2.75	3.92	3.21	4.38	3.23	4.77	3.25
	M3B	2.96	2.06	3.56	2.09	4.07	2.11	4.51	2.14	3.55	2.67	4.06	2.69	4.49	2.72
	M4	4.74	4.07	5.11	4.09	5.41	4.12	5.66	4.14	5.09	4.42	5.39	4.44	5.64	4.46
	M5	4.35	3.74	4.83	3.93	5.07	3.95	5.26	3.97	4.63	4.02	4.88	4.04	5.08	4.06
	M6	3.83	3.34	4.10	3.36	4.32	3.37	4.51	3.39	4.09	3.59	4.31	3.61	4.50	3.62
	M7	1.52	0.77	1.95	0.80	2.31	0.82	2.61	0.85	1.93	1.20	2.29	1.22	2.59	1.25

Table VII.2 Reliability indices for FM1 and FM2 for SG8 to SG13 for M1 to M7 with varying degrees of saturation when H_w = 1.0m

S_r	Model	Reliability Index (β) when H_w = 1.0 m											
		SG8		SG9		SG10		SG11		SG12		SG13	
		FM1	FM2	FM1	FM2	FM1	FM2	FM1	FM2	FM1	FM2	FM1	FM2
%		β_{up}	β_{dwn}	β_{up}	β_{dwn}	β_{up}	β_{dwn}	β_{up}	β_{dwn}	β_{up}	β_{dwn}	β_{up}	β_{dwn}
56.0 - 59.4	M1	2.67	2.43	2.90	2.00	3.06	2.46	2.67	2.61	2.87	2.62	2.67	2.43
	M2	4.17	3.83	4.50	3.85	4.77	3.86	4.16	4.07	4.49	4.09	4.17	3.83
	M3A	3.95	3.65	4.40	3.67	4.79	3.69	3.93	4.01	4.39	4.03	3.95	3.65
	M3B	3.61	3.19	4.12	3.21	4.55	3.23	3.60	3.60	4.11	3.63	3.61	3.19
	M4	5.09	4.66	5.38	4.68	5.63	4.70	5.08	4.87	5.37	4.89	5.09	4.66
	M5	4.63	4.20	4.86	4.22	5.22	4.39	4.61	4.37	5.02	4.53	4.63	4.20
	M6	4.08	3.78	4.30	3.79	4.48	3.80	4.07	3.93	4.29	3.95	4.08	3.78
	M7	1.93	1.53	2.29	1.55	2.59	1.57	1.92	1.83	2.28	1.85	1.93	1.53
72.0 - 76.5	M1	2.66	2.43	2.89	2.00	3.05	2.46	2.66	2.61	2.86	2.62	2.66	2.43
	M2	4.17	3.83	4.49	3.85	4.77	3.87	4.15	4.07	4.48	4.09	4.17	3.83
	M3A	3.93	3.64	4.38	3.66	4.77	3.68	3.92	4.00	4.37	4.02	3.93	3.64
	M3B	3.57	3.17	4.08	3.20	4.51	3.22	3.56	3.59	4.07	3.62	3.57	3.17
	M4	5.08	4.67	5.39	4.69	5.62	4.71	5.07	4.88	5.37	4.90	5.08	4.67
	M5	4.62	4.21	4.86	4.23	5.23	4.40	4.61	4.38	5.02	4.55	4.62	4.21
	M6	4.08	3.78	4.30	3.80	4.48	3.81	4.07	3.94	4.29	3.95	4.08	3.78
	M7	1.92	1.53	2.28	1.56	2.58	1.58	1.91	1.83	2.27	1.85	1.92	1.53
86.5 - 89.8	M1	2.65	2.43	2.88	2.00	3.04	2.46	2.65	2.61	2.85	2.62	2.65	2.43
	M2	4.16	3.83	4.49	3.85	4.76	3.87	4.15	4.07	4.48	4.09	4.16	3.83
	M3A	3.91	3.64	4.37	3.66	4.76	3.68	3.90	4.00	4.36	4.02	3.91	3.64
	M3B	3.54	3.16	4.05	3.19	4.48	3.21	3.52	3.58	4.03	3.60	3.54	3.16
	M4	5.08	4.68	5.38	4.70	5.62	4.72	5.06	4.89	5.36	4.91	5.08	4.68
	M5	4.62	4.22	4.86	4.24	5.23	4.42	4.61	4.39	5.02	4.56	4.62	4.22
	M6	4.08	3.79	4.30	3.80	4.49	3.81	4.07	3.94	4.29	3.96	4.08	3.79
	M7	1.91	1.54	2.27	1.56	2.58	1.58	1.90	1.83	2.26	1.85	1.91	1.54

Table VII.3 Reliability indices for FM1 and FM2 for SG1 to SG7 for M1 to M7 with varying degrees of saturation when H_w = 1.5m

Sr	Model	Reliability Index (β) when H_w = 1.5 m													
		SG1		SG2		SG3		SG4		SG5		SG6		SG7	
		FM1	FM2	FM1	FM2	FM1	FM2	FM1	FM2	FM1	FM2	FM1	FM2	FM1	FM2
%		β_{up}	β_{dwn}	β_{up}	β_{dwn}	β_{up}	β_{dwn}	β_{up}	β_{dwn}	β_{up}	β_{dwn}	β_{up}	β_{dwn}	β_{up}	β_{dwn}
56.0 - 59.4	M1	2.26	1.58	2.52	1.62	2.74	1.65	2.93	1.68	2.50	1.86	2.72	1.89	2.91	1.91
	M2	3.52	2.74	3.90	2.77	4.20	2.80	4.45	2.83	3.87	3.10	4.17	3.13	4.43	3.16
	M3A	3.16	2.19	3.70	2.23	4.14	2.27	4.51	2.30	3.67	2.71	4.11	2.75	4.48	2.78
	M3B	2.77	1.45	3.38	1.50	3.89	1.55	4.32	1.59	3.34	2.06	3.85	2.11	4.28	2.15
	M4	4.42	3.57	4.76	3.61	5.03	3.64	5.25	3.67	4.73	3.90	5.00	3.93	5.22	3.97
	M5	4.28	3.54	4.55	3.57	4.77	3.60	4.94	3.63	4.52	3.80	4.74	3.83	4.92	3.85
	M6	3.59	3.02	3.85	3.04	4.05	3.06	4.22	3.09	3.82	3.26	4.03	3.28	4.20	3.30
	M7	1.16	0.11	1.61	0.17	1.98	0.21	2.31	0.26	1.58	0.56	1.95	0.61	2.28	0.65
72.0 - 76.5	M1	2.24	1.59	2.51	1.62	2.73	1.65	2.92	1.68	2.49	1.86	2.71	1.89	2.90	1.92
	M2	3.51	2.74	3.89	2.77	4.19	2.80	4.45	2.83	3.86	3.10	4.17	3.13	4.42	3.16
	M3A	3.14	2.18	3.68	2.22	4.12	2.26	4.49	2.29	3.65	2.71	4.09	2.74	4.46	2.78
	M3B	2.72	1.44	3.34	1.49	3.85	1.54	4.28	1.58	3.30	2.05	3.81	2.10	4.25	2.14
	M4	4.41	3.57	4.75	3.61	5.02	3.65	5.24	3.68	4.72	3.91	4.99	3.94	5.21	3.97
	M5	4.27	3.55	4.54	3.58	4.76	3.61	4.94	3.63	4.52	3.81	4.74	3.84	4.92	3.86
	M6	3.59	3.02	3.84	3.04	4.05	3.07	4.22	3.09	3.82	3.26	4.03	3.28	4.20	3.30
	M7	1.15	0.12	1.60	0.17	1.97	0.22	2.29	0.27	1.56	0.57	1.94	0.62	2.26	0.66
86.5 - 89.8	M1	2.23	1.59	2.50	1.63	2.72	1.65	2.90	1.68	2.48	1.87	2.70	1.90	2.89	1.92
	M2	3.50	2.73	3.88	2.77	4.19	2.80	4.44	4.44	3.85	3.10	4.16	3.13	4.41	3.16
	M3A	3.13	2.18	3.67	2.22	4.11	2.26	4.49	2.29	3.64	2.71	4.08	2.74	4.46	2.77
	M3B	2.68	1.42	3.29	1.48	3.81	1.52	4.24	1.57	3.26	2.04	3.77	2.09	4.21	2.13
	M4	4.40	3.58	4.74	3.61	5.02	3.65	5.24	3.68	4.71	3.91	4.99	3.95	5.21	3.98
	M5	4.26	3.55	4.54	3.58	4.76	3.61	4.94	3.64	4.51	3.82	4.74	3.84	4.92	3.87
	M6	3.58	3.02	3.84	3.04	4.04	3.07	4.22	3.09	3.81	3.26	4.02	3.28	4.20	3.30
	M7	1.15	0.13	1.59	0.18	1.96	0.23	2.28	0.27	1.56	0.58	1.93	0.62	2.26	0.66

Table VII.4 Reliability indices for FM1 and FM2 for SG8 to SG13 for M1 to M7 with varying degrees of saturation when H_w = 1.5m

Sr	Model	Reliability Index (β) when H_w = 1.5 m											
		SG8		SG9		SG10		SG11		SG12		SG13	
		FM1	FM2	FM1	FM2	FM1	FM2	FM1	FM2	FM1	FM2	FM1	FM2
%		β_{up}	β_{dwn}	β_{up}	β_{dwn}	β_{up}	β_{dwn}	β_{up}	β_{dwn}	β_{up}	β_{dwn}	β_{up}	β_{dwn}
56.0 - 59.4	M1	2.49	2.07	2.71	2.10	2.90	2.12	2.47	2.26	2.70	2.29	2.89	2.31
	M2	3.84	3.37	4.15	3.40	4.40	3.42	3.82	3.60	4.13	3.62	4.38	3.65
	M3A	3.64	3.12	4.08	3.15	4.45	3.18	3.62	3.46	4.06	3.49	4.43	3.52
	M3B	3.31	2.54	3.82	2.58	4.25	2.62	3.28	2.94	3.79	2.99	4.23	3.02
	M4	4.70	4.14	4.97	4.17	5.19	4.20	4.68	4.34	4.94	4.37	5.16	4.40
	M5	4.50	3.98	4.71	4.01	4.89	4.03	4.48	4.13	4.69	4.16	4.87	4.18
	M6	3.81	3.43	4.01	3.45	4.18	3.47	3.79	3.58	4.00	3.60	4.17	3.62
	M7	1.55	0.91	1.93	0.95	2.25	0.99	1.52	1.21	1.90	1.25	2.23	1.29
72.0 - 76.5	M1	2.47	2.08	2.70	2.10	2.89	2.13	2.46	2.26	2.68	2.29	2.88	2.31
	M2	3.84	3.37	4.14	3.40	4.40	3.43	3.82	3.60	4.12	3.63	4.38	3.65
	M3A	3.62	3.11	4.06	3.15	4.44	3.18	3.60	3.46	4.04	3.49	4.41	3.52
	M3B	3.27	2.53	3.78	2.57	4.22	2.61	3.24	2.94	3.76	2.98	4.19	3.02
	M4	4.69	4.15	4.96	4.18	5.19	4.21	4.67	4.34	4.94	4.38	5.16	4.41
	M5	4.49	3.99	4.71	4.02	4.89	4.05	4.47	4.15	4.69	4.17	4.87	4.20
	M6	3.80	3.43	4.01	3.46	4.18	3.48	3.79	3.58	3.99	3.60	4.16	3.62
	M7	1.54	0.91	1.91	0.96	2.24	1.00	1.51	1.22	1.89	1.26	2.22	1.29
86.5 - 89.8	M1	2.46	2.08	2.69	2.10	2.88	2.13	2.45	2.27	2.67	2.29	2.86	2.31
	M2	3.83	3.37	4.13	3.40	4.39	3.43	3.81	3.60	4.11	3.63	4.37	3.66
	M3A	3.61	3.11	4.06	3.15	4.43	3.18	3.59	3.46	4.03	3.49	4.41	3.52
	M3B	3.23	2.52	3.75	2.57	4.18	2.61	3.21	2.93	3.72	2.98	4.16	3.01
	M4	4.69	4.15	4.96	4.19	5.18	4.22	4.66	4.35	4.94	4.39	5.16	4.42
	M5	4.49	4.00	4.71	4.03	4.90	4.06	4.47	4.16	4.69	4.19	4.88	4.21
	M6	3.80	3.44	4.00	3.46	4.18	3.48	3.78	3.59	3.99	3.61	4.16	3.63
	M7	1.53	0.92	1.91	0.96	2.23	1.00	1.51	1.22	1.88	1.26	2.21	1.30

Table VII.5 Reliability indices for FM1 and FM2 for SG1 to SG7 for M1 to M7 with varying degrees of saturation when H_w = 2.0 m

Sr	Model	Reliability Index (β) when H_w = 2.0 m													
		SG1		SG2		SG3		SG4		SG5		SG6		SG7	
		FM1	FM2	FM1	FM2	FM1	FM2	FM1	FM2	FM1	FM2	FM1	FM2	FM1	FM2
%		β_{up}	β_{dwn}	β_{up}	β_{dwn}	β_{up}	β_{dwn}	β_{up}	β_{dwn}	β_{up}	β_{dwn}	β_{up}	β_{dwn}	β_{up}	β_{dwn}
56.0 - 59.4	M1	2.00	1.02	2.28	1.08	2.52	1.12	2.73	1.17	2.25	1.33	2.49	1.37	2.70	1.41
	M2	3.19	2.24	3.54	2.28	3.82	2.32	4.05	2.36	3.50	2.59	3.78	2.63	4.01	2.66
	M3A	2.82	1.55	3.32	1.61	3.74	1.66	4.08	1.70	3.27	2.07	3.69	2.12	4.03	2.16
	M3B	2.39	0.61	2.98	0.68	3.48	0.74	3.89	0.80	2.92	1.22	3.41	1.29	3.83	1.34
	M4	4.00	2.97	4.31	3.02	4.55	3.07	4.74	3.11	4.26	3.30	4.50	3.34	4.69	3.38
	M5	3.82	2.93	4.06	2.97	4.26	3.01	4.41	3.05	4.02	3.18	4.22	3.22	4.37	3.26
	M6	3.33	2.65	3.56	2.68	3.75	2.71	3.91	2.74	3.53	2.89	3.72	2.91	3.88	2.94
	M7	0.67	-0.76	1.13	-0.68	1.53	-0.61	1.87	-0.54	1.08	-0.29	1.47	-0.22	1.81	-0.16
72.0 - 76.5	M1	1.98	1.03	2.27	1.09	2.51	1.13	2.71	1.18	2.23	1.33	2.47	1.38	2.68	1.42
	M2	3.18	2.24	3.53	2.28	3.81	2.32	4.04	2.35	3.49	2.59	3.77	2.63	4.00	2.66
	M3A	2.79	1.55	3.30	1.60	3.72	1.65	4.07	1.70	3.25	2.07	3.67	2.11	4.02	2.16
	M3B	2.34	0.60	2.94	0.67	3.44	0.73	3.85	0.79	2.88	1.22	3.38	1.28	3.79	1.34
	M4	3.99	2.97	4.30	3.02	4.54	3.07	4.73	3.11	4.25	3.30	4.49	3.35	4.69	3.39
	M5	3.81	2.94	4.06	2.98	4.25	3.02	4.41	3.05	4.02	3.19	4.21	3.23	4.37	3.26
	M6	3.33	2.65	3.56	2.68	3.75	2.71	3.90	2.74	3.53	2.89	3.72	2.91	3.87	2.94
	M7	0.66	-0.74	1.12	-0.67	1.51	-0.60	1.85	-0.53	1.06	-0.28	1.46	-0.21	1.80	-0.15
86.5 - 89.8	M1	1.97	1.04	2.25	1.09	2.49	1.14	2.70	1.19	2.22	1.34	2.46	1.39	2.67	1.43
	M2	3.17	2.24	3.52	2.28	3.80	2.32	4.03	2.35	3.48	2.59	3.76	2.63	3.99	2.66
	M3A	2.78	1.55	3.29	1.60	3.71	1.65	4.06	1.70	3.24	2.06	3.66	2.11	4.01	2.16
	M3B	2.29	0.59	2.90	0.66	3.40	0.72	3.82	0.78	2.83	1.21	3.34	1.27	3.76	1.33
	M4	3.98	2.98	4.29	3.03	4.53	3.07	4.73	3.12	4.24	3.31	4.49	3.35	4.68	3.39
	M5	3.80	2.94	4.05	2.98	4.24	3.02	4.40	3.06	4.01	3.20	4.20	3.23	4.36	3.27
	M6	3.32	2.65	3.55	2.68	3.74	2.71	3.90	2.74	3.52	3.52	3.71	2.91	3.87	2.94
	M7	0.65	-0.74	1.11	-0.66	1.50	-0.59	1.84	-0.52	1.05	-0.27	1.45	-0.20	1.79	-0.14

Table VII.6 Reliability indices for FM1 and FM2 for SG8 to SG13 for M1 to M7 with varying degrees of saturation when H_w = 2.0 m

Sr	Model	Reliability Index (β)when H_w = 2.0 m											
		SG8		SG9		SG10		SG11		SG12		SG13	
		FM1	FM2	FM1	FM2	FM1	FM2	FM1	FM2	FM1	FM2	FM1	FM2
%		β_{up}	β_{dwn}	β_{up}	β_{dwn}	β_{up}	β_{dwn}	β_{up}	β_{dwn}	β_{up}	β_{dwn}	β_{up}	β_{dwn}
56.0 - 59.4	M1	2.22	1.55	2.46	1.59	2.67	1.63	2.19	1.75	2.44	1.79	2.65	1.82
	M2	3.46	2.85	3.78	2.63	3.98	2.92	3.43	3.07	3.71	3.10	3.95	3.13
	M3A	3.23	2.46	3.65	2.50	3.99	2.54	3.19	2.79	3.61	2.83	3.95	2.87
	M3B	2.86	1.69	3.36	1.75	3.77	1.80	2.81	2.09	3.31	2.14	3.72	2.19
	M4	4.22	3.53	4.46	3.57	4.65	3.60	4.19	3.72	4.43	3.75	4.62	3.79
	M5	3.99	3.36	4.18	3.39	4.34	3.43	3.96	3.50	4.15	3.54	4.31	3.57
	M6	3.51	3.05	3.70	3.08	3.86	3.10	3.49	3.19	3.68	3.22	3.83	3.24
	M7	1.03	0.06	1.42	0.12	1.77	0.18	0.98	0.37	1.38	0.43	1.73	0.48
72.0 - 76.5	M1	2.20	1.56	2.45	1.60	2.66	1.63	2.18	1.75	2.42	1.79	2.64	1.83
	M2	3.45	2.85	3.77	2.63	3.97	2.92	3.42	3.07	3.71	3.10	3.94	3.13
	M3A	3.21	2.46	3.63	2.50	3.97	2.54	3.17	2.79	3.59	2.83	3.94	2.87
	M3B	2.82	1.69	3.32	1.74	3.74	1.80	2.77	2.09	3.27	2.14	3.69	2.19
	M4	4.21	3.53	4.45	3.57	4.65	3.61	4.18	3.73	4.42	3.76	4.62	3.80
	M5	3.98	3.37	4.18	3.40	4.34	3.43	3.95	3.51	4.15	3.55	4.31	3.58
	M6	3.50	3.05	3.69	3.08	3.85	3.10	3.48	3.20	3.67	3.22	3.83	3.24
	M7	1.01	0.07	1.41	0.13	1.75	0.19	0.97	0.38	1.37	0.44	1.71	0.49
86.5 - 89.8	M1	2.19	1.56	2.43	1.60	2.64	1.64	2.16	1.76	2.41	1.80	2.62	1.83
	M2	3.44	2.85	3.76	2.63	3.96	2.92	3.41	3.07	3.70	3.10	3.93	3.14
	M3A	3.20	2.46	3.62	2.50	3.97	2.54	3.16	2.79	3.58	2.83	3.93	2.87
	M3B	2.78	1.68	3.28	1.74	3.71	1.79	2.74	2.09	3.24	2.14	3.66	2.19
	M4	4.20	3.54	4.45	3.58	4.64	3.62	4.17	3.73	4.41	3.77	4.61	3.81
	M5	3.97	3.37	4.17	3.41	4.33	3.44	3.95	3.52	4.14	3.56	4.30	3.59
	M6	3.49	3.06	3.69	3.08	3.84	3.11	3.47	3.20	3.66	3.22	3.82	3.25
	M7	1.00	0.08	1.40	0.14	1.74	0.20	0.96	0.39	1.36	0.44	1.70	0.50

APPENDIX VIII : UK CLIMATE VARIABLES AND MODELLING OF DAM SCENARIOS UNDER VARYING PRECIPITATION PATTERNS

This appendix contains the tables showing the relationship between the different UK common climate variables and the how selected global climate change variables directly influence UK primary and synoptic climate variables.

VIII.1 UK Common Climate Variables

Table VIII.1 shows the relationship between the different UK common climate variables defined as primary, synoptic, compound and proxy climate variables. From the table it is possible to ascertain the relationship between the primary, synoptic, compound and proxy climate variables. Table VIII.2 demonstrates how selected global climate change variables directly influence the UK primary and synoptic climate variables.

Table VIII.1 Relationship between the primary, synoptic, compound and proxy UK common climate variables

			UK Common Climate Variables															
			Synoptic							Compound					Proxy			
			Weather types	Storm tracks	Pressure	Pressure gradient	Ocean/ Marine climatology	Moisture content in air/material/ etc…	Lightning	Evapo-transpiration	Marine climate	Relative humidity	Relative mist and fog	Growing season	Soil Moisture	Wave climate	Water run-off	Seasonality variability
UK Common Climate Variables	**Primary**	Temperature	*	*	*	*	*	*	*	*		*	*	*	*			*
		Precipitation	*	*	*	*	*	*	*	*				*	*		*	*
		Snowfall	*	*	*	*	*	*		*				*	*		*	*
		Wind	*	*	*	*	*	*		*	*	*	*			*	*	*
		Cloud cover	*	*	*	*	*			*			*	*	*			*
		Sea level	*				*				*					*		*
		Carbon dioxide	*		*	*	*	*	*					*				*
	Synoptic	Weather types									*				*			*
		Storm tracks									*				*			
		Pressure		*		*	*	*	*		*	*						
		Pressure gradient		*			*	*	*		*							
		Ocean/Marine/ climatology	*						*		*					*		
		Moisture content in the air/material/etc..								*	*	*			*			
		Lightning	*	*							*							
	Compound	Evapo-transpiration															*	*
		Marine climate														*		*
		Relative humidity													*			*
		Relative mist and fog													*			*
		Growing season													*		*	*

** shows relationship between the UK common climate variables*

Table VIII.2 Relationship between selected global climate change variables and UK primary and synoptic climate variables

				UK Common Climate Variables														
				Primary							Synoptic							
				Temperature	Precipitation	Snowfall	Wind	Cloud cover	Sea level	Carbon dioxide	Weather types	Storm tracks	Pressure	Pressure gradient	Ocean/ Marine climatology	Moisture content in the air/material/ etc.	Lightning
Global Climate Change	**Man-made Causes**		Greenhouse gases	*		*				*							
			Aerosols	*						*							
			Radioactive forcing							*							
			Changes in land use							*							
	Natural Causes	**Natural factors**	Solar variations	*				*			*		*	*		*	
			Orbital variations						*		*						
			Volcanism						*	*							
			Seismic effects								*						
		Natural processes	Glacial variations	*	*				*		*				*	*	
			Ocean variability	*	*				*							*	
			Ocean and atmosphere interactions	*	*	*	*				*	*	*		*	*	*

** shows relationship between the UK common climate variables*

APPENDIX IX : APPLICATION OF THE UKCP09 USER INTERFACE

This appendix shows the application of the UKCP09 User Interface used to predict the probable future rainfall intensities for January and July between 2010 - 2039 and 2070 = 2099.

IX.1 Probable Future Rainfall Intensities Derived Using UKCP09

The UKCP09 User Interface combines the probabilistic climate change projections with the precipitation recorded during the baseline period (1961 - 1990). Here, the UKCP09 climate projections for High Emission (A1FI) Scenarios and the Cumulative Distribution Function (CDF) are plotted. Figure IX.1 shows the CDF of the projected change in precipitation for high emission (A1FI) scenarios, for the London region, for January and July between 2010 - 2039 and 2070 - 2099.

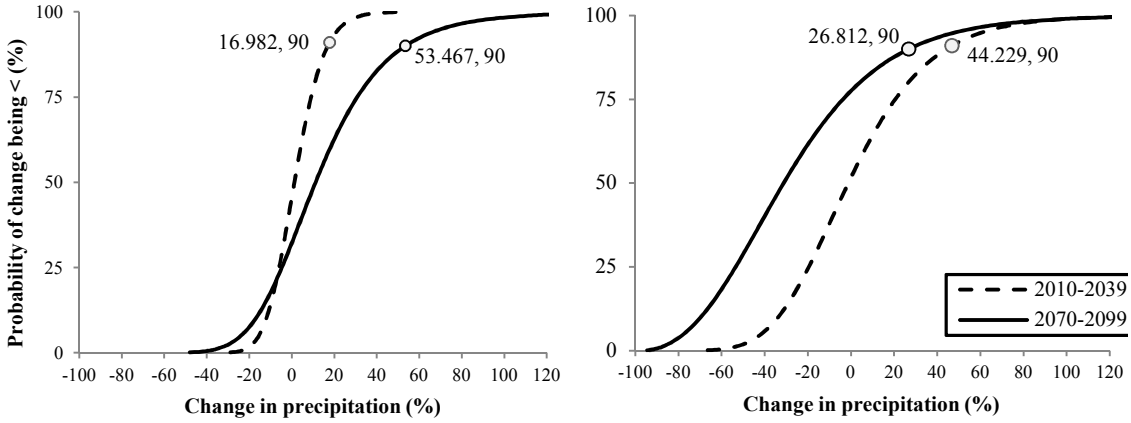

(January) (July)

Figure IX.1 CDF of change in precipitation for high emission (A1FI) scenario: London region[4]

Before the probable future rainfall intensity for January and July between 2010 - 2039 and 2070 - 2099 are obtained, their future rainfall intensities must be calculated. This is carried out by first identifying the change in precipitation (%), for high emission (A1FI) scenarios, for a given probability level. Here, the 90% probability level is selected and the percentage change in precipitation obtained from the CDF graphs in Figure IX.1. The next step is to determine the month's average or mean rainfall intensity (μ_{RI}) recorded over the baseline (1961 - 1990).

Once the mean rainfall intensity is obtained, the future average rainfall intensity (μ_{FRI}) over a 30 year period can be estimated. This is calculated by multiplying the month's average rainfall intensity recorded over the baseline (1961 - 1990) with the percentage increase of the change in precipitation for the selected 30 year period.

$$\mu_{FRI} = \mu_{RI}\left(\frac{100 + x_{\text{percentage of the change in precipitation}}}{100}\right) \quad \text{(IX.1)}$$

Lastly, the variance and standard deviation for the future rainfall intensity are obtained, Eqns. (IX.1 and IX.2).

$$\text{Variance} = \sigma^2 = \frac{1}{n}\sum_{i=1}^{n}\left(x_i - \mu_{FRI}\right)^2 \quad \text{(IX.2)}$$

$$\text{Standard Deviation } = \sigma = \sqrt{variance} \quad \text{(IX.3)}$$

[4] Source: UKCP09 User Interface

Table IX.1 shows the recorded and predicted future rainfall intensities calculated for January and July over the baseline and between 2010 - 2039 and 2070 - 2099 using the above equations and their UKCP09 change in precipitation obtained from the CDF graphs in Figure IX.1.

Table IX.1 Recorded and predicted rainfall intensities calculated for January and July over the baseline and between 2010 - 2039 and 2070 - 2099 using the UKCP09 User Interface

Month and 30 Year Period		Units	January	July
(Baseline) 1961 - 1990	Total RI	mm	2298.40	1434.70
	Average RI		79.26	49.47
2010 - 2039	UKCP09 change in precipitation*	%	16.98	44.23
	Future average RI (μ_{FRI})	mm	92.71	71.35
	Variance (σ^2)		1725.58	1008.88
	Standard Deviation (σ)		41.54	31.76
2070 - 2099	UKCP09 change in precipitation*	%	53.47	26.81
	Future average RI (μ_{FRI})	mm	121.63	62.74
	Variance (σ^2)		3553.83	666.20
	Standard Deviation (σ)		59.61	25.81

**UKCP09 change in precipitation at 90% probability level (see graphs in Figure IX.1)*

Once the mean and standard deviation for the future rainfall intensity for January and July between 2010 - 2039 and 2070 - 2099 are equated, the month's probable future rainfall intensity over a 30 year period can be ascertained. Table IX.2 shows the calculated probable future rainfall intensities for the 95th fractile ($<\mu>_{1\text{-}0.95}$). These were then incorporated into the probabilistic model, as implemented in *Chapter 6: Subsection 6.2.2.1*.

Table IX.2 Probable future rainfall intensities incorporating UKCP09 climate projections

Month and 30 year period	μ_{FRI}	σ	$\left(\frac{\sigma}{1}\right) \cdot 1.96^{**}$	$<\mu>_{1\text{-}0.95}$	Rainfall Duration	Average Rainfall Rate
January 2010 - 2039	92.71	41.54	81.42	174.13	31days	5.62 mm/day
January 2070 - 2099	71.35	31.76	62.26	133.61	31days	7.69 mm/day
July 2010 - 2039	121.63	59.61	116.84	238.47	1hr	133.61 mm/hr
July 2070 - 2099	62.74	25.81	50.59	113.33	1hr	113.33 mm/hr

***Extracted from the CDF for standard normal distribution table by Haldar and Mahadevan (2000)*